

Online Research @ Cardiff

This is an Open Access document downloaded from ORCA, Cardiff University's institutional repository: <http://orca.cf.ac.uk/129211/>

This is the author's version of a work that was submitted to / accepted for publication.

Citation for final published version:

Petersen, Jan, Ciacchi, Laura, Tran, Mai T., Loh, Khai Lee, Kooy-Winkelaar, Yvonne, Croft, Nathan P., Hardy, Melinda Y., Chen, Zhenjun, McCluskey, James, Anderson, Robert P., Purcell, Anthony W., Tye-Din, Jason A., Koning, Frits, Reid, Hugh H. and Rossjohn, Jamie 2020. T cell receptor cross-reactivity between gliadin and bacterial peptides in celiac disease. *Nature Structural and Molecular Biology* 27 (1) , pp. 49-61. 10.1038/s41594-019-0353-4 file

Publishers page: <http://dx.doi.org/10.1038/s41594-019-0353-4> <<http://dx.doi.org/10.1038/s41594-019-0353-4>>

Please note:

Changes made as a result of publishing processes such as copy-editing, formatting and page numbers may not be reflected in this version. For the definitive version of this publication, please refer to the published source. You are advised to consult the publisher's version if you wish to cite this paper.

This version is being made available in accordance with publisher policies. See <http://orca.cf.ac.uk/policies.html> for usage policies. Copyright and moral rights for publications made available in ORCA are retained by the copyright holders.



1 **T cell receptor cross-reactivity between gliadin and bacterial peptides in celiac**
2 **disease**

3
4 Jan Petersen^{1,2}, Laura Ciacchi^{1,2}, Mai T. Tran¹, Khai-Lee Loh¹, Yvonne Kooy-Winkelaar³, Nathan
5 P. Croft¹, Melinda Y. Hardy^{4,5}, Zhenjun Chen⁶, James McCluskey⁶, Robert P. Anderson⁷, Anthony
6 W. Purcell¹, Jason A. Tye-Din^{4,5,8}, Frits Koning³, Hugh H. Reid^{1,2*} & Jamie Rossjohn^{1,2,9*}
7

8 ¹Infection and Immunity Program and The Department of Biochemistry and Molecular Biology,
9 Biomedicine Discovery Institute Monash University, Clayton, Victoria 3800, Australia.

10 ²Australian Research Council Centre of Excellence in Advanced Molecular Imaging, Monash
11 University, Clayton, Victoria 3800, Australia.

12 ³Department of Immunohematology and Blood Transfusion, Leiden University Medical Center,
13 Leiden 2333 ZA, The Netherlands.

14 ⁴The Walter and Eliza Hall Institute of Medical Research, 1G Royal Parade, Parkville, Victoria
15 3052, Australia.

16 ⁵Department of Medical Biology, The University of Melbourne, Parkville, Victoria 3052, Australia.
17

18 ⁶Department of Microbiology & Immunology, Peter Doherty Institute for Infection and Immunity,
19 University of Melbourne, Melbourne, Victoria 3010, Australia

20 ⁷ImmusanT, Inc., One Kendall Square, Suite B2004, Cambridge, MA 02139, USA
21

22 ⁸Department of Gastroenterology, The Royal Melbourne Hospital, Parkville, Victoria 3052,
23 Australia.

24 ⁹Institute of Infection and Immunity, Cardiff University School of Medicine, Heath Park, Cardiff
25 CF14 4XN, UK.
26

27 * joint senior & corresponding authors. hugh.reid@monash.edu and jamie.rossjohn@monash.edu
28

29 *Running title: Molecular mimicry in Celiac Disease*
30
31
32

37 **The *Human Leukocyte Antigen (HLA) locus* is strongly associated with T cell mediated**
38 **autoimmune disorders. HLA-DQ2.5-mediated celiac disease (CeD) is triggered by ingestion of**
39 **gluten, although the relative role of genetic and environmental risk factors in CeD is unclear.**
40 **Here we identify microbially-derived mimics of gliadin epitopes and a parental bacterial**
41 **protein that is naturally processed by antigen presenting cells and activated gliadin-reactive**
42 **HLA-DQ2.5 restricted T cells derived from CeD patients. Crystal structures of T cell**
43 **receptors (TCRs) in complex with HLA-DQ2.5 bound to two distinct bacterial peptides**
44 **demonstrate that molecular mimicry underpins cross-reactivity towards the gliadin epitopes.**
45 **Accordingly, gliadin reactive T cells involved in CeD pathogenesis cross-react with ubiquitous**
46 **bacterial peptides, thereby suggesting microbial exposure as a potential environmental factor**
47 **in CeD.**

48

49 **Introduction**

50 The ability of T cells to distinguish between self- and non-self is determined by T cell receptors
51 (TCRs) on the surface of T cells recognising peptides bound to Human Leukocyte Antigen (HLA)
52 molecules. However, failure of self/non-self discrimination may cause aberrant T cell reactivity
53 against self-peptides and the manifestation of immune-mediated inflammatory diseases (IMID).
54 However, the factors leading to T cell autoimmunity remain obscure.

55

56 The *Human Leukocyte Antigen Class II (HLA-II) locus* represents an important genetic determinant
57 in IMIDs¹. Nevertheless, the molecular mechanism underpinning this genetic linkage for the vast
58 majority of IMIDs are unclear. The HLA-bound peptides that precipitate autoimmunity are often
59 unknown and it is unclear why tolerance is broken². Moreover, there is a poor understanding of the
60 T cell repertoire directed towards autoreactive peptide-HLA complexes. Notably, the non-HLA
61 linked genetic risk is generally thought to be multi-factorial and shared between different IMIDs,
62 with several lines of evidence implying that environmental factors are likely to play an important
63 role as well. Disease associations with major environmental risk factors are much more diffuse and
64 include the exposure to toxic chemicals³, the dysregulation of the gut microbiota⁴ and certain
65 infections⁵. However, the relative contributions and mechanisms governing environmental and
66 genetic risk factors in autoimmunity and autoimmune-like disorders remain unclear.

67

68 To begin to address these central questions regarding IMIDs, we have investigated the molecular
69 mechanisms of the CD4⁺ T cell response in Celiac Disease (CeD), as the nature of the antigens that
70 triggers the disease is well established⁶⁻⁸. CeD is a T cell mediated IMID that is caused by an
71 environmental antigen, dietary gluten. CeD is essentially restricted to genetically predisposed

72 individuals, namely those who are HLA-DQ2.5⁺ and/or HLA-DQ8⁺. Approximately 95% of CeD
73 patients carry HLA-DQ2.5 (alleles *DQA1**05:01 and *DQB1**02:01), and the majority of HLA-
74 DQ2.5⁻ patients express HLA-DQ8 (alleles *DQA1**03:01 and *DQB1**03:02)⁶. In CeD, gluten
75 peptide deamidation by tissue transglutaminase 2 (TG2) strengthens binding of epitopes to these
76 disease-associated HLA molecules^{9,10}, thereby increasing both antigen presentation, and the
77 recognition by gluten-specific CD4⁺ T cells¹¹⁻¹⁴. T cell activity in HLA-DQ2.5-associated CeD is
78 targeted towards gluten peptides originating from wheat, rye or barley. In relation to wheat, the
79 immunodominant deamidated gluten peptide encompasses two overlapping T cell determinants in
80 wheat gliadin (DQ2.5-glia- α 1a, PFPQPELPY, and DQ2.5-glia- α 2: PQPELPYPQ). HLA-DQ2.5-
81 mediated CeD is characterised by biased TCR usage¹²⁻¹⁵. T cells expressing TRAV26-1 and
82 TRBV7-2 predominate in the HLA-DQ2.5-glia- α 2 specific T cell response while HLA-DQ2.5-glia-
83 α 1a restricted TCRs show biased usage of TRBV29-1 genes. The HLA-DQ2.5-glia- α 2 specific T
84 cell response is also characterised by an arginine residue in the CDR3 loop, which plays a key role
85 in TCR recognition. Crystal structures of a TRAV4/TRBV20-1⁺ TCR-DQ2.5-glia- α 1a complex and
86 TRAV26-1/TRBV7-2⁺ TCR-HLA-DQ2.5-glia- α 2 complexes provided a molecular mechanism
87 underpinning these epitope specificities and the HLA-DQ2.5-glia- α 2 restricted TCR bias¹⁴.

88

89 However, while the role of HLA-DQ2 and HLA-DQ8 in the presentation of gluten epitopes is clear,
90 the presence of these *HLA* alleles is insufficient to cause disease, as the *HLA* penetrance for this
91 disease is no more than 3%⁶, and age of onset is at a median of 3 years and rarely before the second
92 year of life¹⁶. Thus, other genetic and environmental factors must contribute to disease
93 development. While epidemiological studies have linked environmental events such as infections
94 with the onset of CeD these cannot establish causality so there is a strong need to understand the
95 mechanistic basis for these observations¹⁷⁻¹⁹. An emerging view is that environmental factors can
96 modify the gut microbiota composition and/or function in genetically susceptible hosts contributing
97 to dysfunctional microbe-host interactions that promote CeD²¹. Reported protein sequence
98 homology between gliadin and adenovirus raised the possibility of molecular mimicry as a
99 contributor to CeD pathogenesis in 1984 but without data supporting an effect in disease relevant T
100 cells this theory was largely disregarded^{20,21}. Here we identify and characterise a number of mimics
101 of HLA-DQ2.5-restricted gliadin determinants derived from common environmental bacteria, and
102 show that they activate disease-relevant, gliadin-reactive T cells isolated from CeD patients. Using
103 structural biology, we show that molecular mimicry underpins this cross-reactive TCR response.
104 Accordingly, our results suggest TCR cross-reactivity between gliadin and microbial peptides in
105 HLA-DQ2.5⁺ individuals is a plausible biological mechanism that supports a potential pathogenic
106 link between some environmentally-derived bacteria and CeD.

107

108 **Results**

109 **Identification of microbial mimic peptides of immunodominant CeD epitopes**

110 To establish whether gliadin reactive T cells could cross-react with structurally similar antigens
111 from bacteria, we searched for microbial peptide sequences that could act as molecular mimics of
112 immunodominant CeD-associated deamidated gliadin epitopes. To reduce the extent of false
113 positive hits from a sequence-only based search, we undertook a structurally-guided database
114 search, using constraints imposed by knowledge of the TCR-HLA-DQ2.5-gliadin crystal structures.
115 Namely, (i) the HLA DQ-2.5 anchor residues at positions P4 (mimics of HLA-DQ2.5 $\text{glia-}\alpha 1\text{a}$ and
116 the related DQ2.5- $\text{glia-}\omega 1$) and P6 (HLA-DQ2.5 $\text{glia-}\alpha 2$ mimics) were fixed to a negatively
117 charged residue (Glu or Asp); (ii) peptides with non-conservative substitutions in positions strictly
118 required for TCR recognition^{14,22} were removed (**Figure 1a**). We searched the NCBI protein
119 database for microbial peptide sequences with high homology to the nine amino-acid core of the
120 immunodominant, deamidated CeD epitopes (DQ2.5- $\text{glia-}\alpha 1\text{a}$ (PFPQPELPY), DQ2.5- $\text{glia-}\omega 1$
121 (PFPQPEQPF) and DQ2.5- $\text{glia-}\alpha 2$ (PQPELPYPQ), and further limited search parameters to
122 microbes commonly associated with infections, the human microbiota, or reported to be in
123 association with CeD. After removing duplicates and homologous sequences with gaps or
124 insertions, we further selected sequences that conformed with the consensus peptide fine specificity
125 of HLA-DQ2.5 restricted T cells from CeD patients (**Figure 1a**)^{14,22}. Among the candidate peptides
126 we noted a set of homologous, overlapping peptides from the *Pseudomonas fluorescens* protein
127 succinylglutamate desuccinylase (PFSGDS), that mimicked the overlapping gliadin epitopes
128 DQ2.5- $\text{glia-}\alpha 1\text{a}$ and DQ2.5- $\text{glia-}\alpha 2$. We selected 23 minimal candidate peptides for further study
129 (**Figure 1b**). These included variants of the overlapping mimic peptides from different *P.*
130 *fluorescens* strains (DQ2.5-*P.fluor-}\alpha 1\text{a}*, *-}\alpha 2\text{a}* and DQ2.5-*P.fluor-}\alpha 1\text{b}* *-}\alpha 2\text{b}*) and four non-bacterial
131 peptides that were identified in archaea and yeast. Accordingly, the structurally-guided database
132 search identified candidate mimics of a number of HLA-DQ2.5-restricted gliadin epitopes.

133

134 **Cross-reactivity between bacterial mimics and gliadin epitopes**

135 To determine the extent of T cell cross-reactivity between each candidate mimic and gliadin
136 epitope, we tested T cell responses using SKW3 cells that had been transduced with TCRs
137 previously characterised from CeD patients. We used the TCRs LS2.8/3.15, N12, L6, JR5.1 and
138 S16, which had established specificities for the CeD epitopes, DQ2.5- $\text{glia-}\alpha 1\text{a}$, DQ2.5- $\text{glia-}\omega 1$ and
139 DQ2.5- $\text{glia-}\alpha 2$ ¹⁴. The candidate peptides were tested in two groups, namely the DQ2.5- $\text{glia-}\alpha 1\text{a}$ /
140 DQ2.5- $\text{glia-}\omega 1$ mimics, and the DQ2.5- $\text{glia-}\alpha 2$ mimics. The DQ2.5- $\text{glia-}\alpha 1\text{a}/\omega 1$ mimics were tested
141 against SKW3.LS2.8/3.15-TCR and SKW3.N12-TCR cell lines, which both recognise DQ2.5- glia-

142 $\alpha 1a$, and against SKW3.L6-TCR cell line that cross-reacts with DQ2.5-glia- $\alpha 1a$ and DQ2.5-glia-
143 $\omega 1$ ²². The DQ2.5-glia- $\alpha 2$ mimics were tested against SKW3.JR5.1-TCR and SKW3.S16-TCR cell
144 lines, whose TCRs express the well-characterised, TRAV26-1/TRBV7-2 biased TCR usage with a
145 conserved arginine within the CDR3 β loop. Stimulation assays established that each T cell line was
146 readily activated by the expected gliadin peptide at 32 $\mu\text{g/ml}$ and responded to at least one of the
147 10- and 11-mer mimic peptides in the presence of HLA-DQ2⁺ antigen presenting cells (**Figure 2**).
148 To obtain a relative measure of potency, we tested T cell line responses in the presence of peptide
149 concentrations ranging from 1 - 32 $\mu\text{g/ml}$ for the DQ2.5-glia- $\alpha 1a/\omega 1$ and DQ2.5-glia- $\alpha 2$ mimics,
150 respectively (**Supplementary Figure 1a and 1b**), and confirmed HLA-DQ restriction by testing T
151 cell line responses in the presence anti-DR, anti-DP and anti-DQ blocking antibodies
152 (**Supplementary Figure 2a**).

153

154 The SKW3.LS2.8/3.15-TCR, SKW3.N12-TCR and SKW3.L6-TCR cell lines responded
155 moderately to the canonical DQ2.5-glia- $\alpha 1a$ epitope at higher concentrations, and only the DQ2.5-
156 glia- $\alpha 1a$ /DQ2.5-glia- $\omega 1$ cross-reactive SKW3.L6-TCR responded to DQ2.5-glia- $\omega 1$ (**Figure 2a**,
157 **Supplementary Figure 1a**). One of the mimic epitopes, DQ2.5-*P.fluor-a1a*, was recognised by all
158 three cell lines and elicited markedly stronger responses in the SKW3.LS2.8/3.15-TCR and
159 SKW3.N12-TCR cell lines than the canonical DQ2.5-glia- $\alpha 1a$ (**Figure 2a**). The T cell response to
160 the related epitope DQ2.5-*P.fluor-a1b*, from a variant *P. fluorescens* strain was similarly strong in
161 the SKW3.N12-TCR cell line, but weaker in the SKW3.LS2.8/3.15-TCR cell line and absent in the
162 SKW3.L6-TCR line. In addition, the SKW3.N12-TCR line responded to DQ2.5-*E.cloac-omega 1a* from
163 *Enterobacter cloacae* at higher concentrations, and the mimic DQ2.5-*A.baum-a1a* from
164 *Acinetobacter baumannii* elicited weak responses in SKW3.L6-TCR and SKW3.N12-TCR (**Figure**
165 **2a, Supplementary Figure 1a**).

166

167 The SKW3.JR5.1-TCR and SKW3.S16-TCR cell lines were strongly activated by DQ2.5-glia- $\alpha 2$,
168 but showed significant differences in their responses to the bacterial mimic peptides. Namely,
169 SKW3.JR5.1-TCR was strongly activated by the mimics DQ2.5-*P.aerug-a2a*, DQ2.5-*P.fluor-a2a*,
170 and by the variant DQ2.5-*P.fluor-a2b*. In contrast, the SKW3.S16-TCR cell line strongly responded
171 to DQ2.5-*B.copro-a2a*, but only marginally responded to DQ2.5-*P.fluor-a2a* and not to DQ2.5-
172 *P.aerug-a2a* or DQ2.5-*P.fluor-a2b* (**Figure 2b, Supplementary Figure 1b**). The discordant
173 specificity of JR5.1 and S16 may be related to how these TCRs differ in their degree of HLA-
174 DQ2.5-glia- $\alpha 2$ engagement¹⁴. Thus, there are distinct patterns of TCR cross-reactivity between
175 distinct gliadin epitopes and the bacterial mimics.

176

177 **The parental bacterial protein is naturally processed and presented**

178 An observation arising from previous stimulation experiments was that, when combined, the
179 overlapping epitopes DQ2.5-glia- α 1a and DQ2.5-glia- α 2 elicited stronger responses in T cell lines.
180 We therefore tested SKW3 T cell activation by longer versions of mimic epitopes (**Supplementary**
181 **Figure 2**) and investigated the parental protein (PFSGDS) from which the overlapping epitopes
182 DQ2.5-*P.fluor- α 1a* and DQ2.5-*P.fluor- α 2a* were derived. The PFSGDS protein was expressed in *E.*
183 *coli* and purified by immobilized metal affinity chromatography followed by gel filtration
184 (**Supplementary Figure 3**). The immunogenicity of the purified PFSGDS protein was
185 subsequently tested in the SKW3.TCR cell line stimulation tests, and several of the lines responded
186 although generally weaker when compared to the 10-mer peptides DQ2.5-*P.fluor- α 1a* and DQ2.5-
187 *P.fluor- α 2a* (**Figure 2 and Supplementary Figure 1**). We reasoned that inefficient stimulation was
188 either due to limited uptake of protein by the B lymphoblastoid cell line (BLCL) used as antigen-
189 presenting cells in this assay (BLCL), or due to inadequate processing and presentation of the full-
190 length protein by HLA-DQ2.5. To exclude the latter possibility, we incubated 0.5×10^9 antigen
191 presenting cells (HLA-DQ2.5⁺ 9022 BLCL, or HLA-DQ8⁺ 9033 BLCL) in the presence of 300
192 μ g/ml of PFSGDS overnight and subsequently isolated cellular HLA-DQ via immunoprecipitation.
193 The bound peptides were eluted and analysed via mass spectrometry as previously described²³.
194 Amongst the HLA-DQ2.5 peptides identified from the antigen fed 9022 BLCL, a single nested set
195 of peptides covering the sequence of both DQ2.5-*P.fluor- α 1a* and DQ2.5-*P.fluor- α 2a* (**Figure 3a**)
196 was detected. In contrast, peptides isolated from antigen –exposed 9033 BLCL expressing HLA-
197 DQ8 produced no such match against the sequence of PFSGDS (**Figure 3a**). To confirm the
198 identity of DQ2.5-*P.fluor- α 1a/2* derived peptides, the chromatographic retention and fragmentation
199 spectra of the synthetic 15-mer peptide derived from this region of DQ2.5-*P.fluor- α 1a/2a* was
200 compared to the relevant experimentally-derived peptide (**Figure 3b, Supplementary Figure 2**).
201 This analysis confirmed that the PFSGDS protein was processed and presented by HLA-DQ2.5⁺
202 BLCL but not by HLA-DQ8⁺ BLCL. Since the 15-mer DQ2.5-*P.fluor- α 1a/2a* peptide includes the
203 two predicted overlapping epitopes, we tested this peptide for recognition by each of the SKW3 T
204 cell lines (**Supplementary Figure 2**). Notably, this peptide elicited strong signals in all
205 SKW3.TCR cell lines tested, including S16, which only marginally responded to DQ2.5-*P.fluor- α 2a*
206 (**Supplementary Figure 1b**). This indicated that SKW3.S16-TCR cell line was sensitive to the
207 overall length of the bacterial mimic peptide. Moreover, these results suggested that the PFSGDS
208 protein is immunogenic for a broad range of T cell lines tested.

209

210 **CeD patient-derived T cells proliferate in response to bacterial peptides**

211 Next, to gauge the immunogenicity of the PFSGDS protein for CeD-associated T cells in a more
212 physiological setting we determined T cell proliferation of CeD patient-derived T cell clones using
213 HLA-DQ2.5⁺ PBMCs as antigen-presenting cells (**Figure 3c**). Overall, 4 of the 9 patient-derived T
214 cell clones were restricted to HLA-DQ2.5-glia- α 1a (25-5101, N10, N12 and L6), and 5 to HLA-
215 DQ2.5-glia- α 2 (S16, 25-5204, 136-009, M402, D1). Moreover, the T cell clones included 3 (N12,
216 L6 and S16) that matched the TCRs of the SKW3 TCR cell lines used in the mimic peptide screen.
217 We measured proliferation via ³H-Thymidine incorporation in response to PFSGDS protein and two
218 13-mer peptides, *DQ2.5-P.fluor- α 1a-13mer* and *DQ2.5-P.fluor- α 2a-13mer*, each containing both 9-
219 mer cores of the mimic epitopes *DQ2.5-P.fluor- α 1a* and *DQ2.5-P.fluor- α 2a* (**Supplementary**
220 **Figure 2**). With the exception of L6, each of the patient-derived T cell clones responded to one or
221 both of the 13-mer mimic peptides with a response comparable to the canonical gliadin peptide, and
222 the majority of TCCs (except L6 and 136-009) responded vigorously to the PFSGDS protein. The T
223 cell clones 25-5101 and N10 failed to respond to *DQ2.5-P.fluor- α 2a* suggesting that both T cell
224 clones required the N-terminally extended core peptide for recognition. We subsequently repeated
225 the experiment for HLA-DQ2.5-glia- α 1a restricted TCCs N10, N12, K5103 and 25-5204 using
226 different concentrations of PFSGDS and peptide (**Figure 3d**) and observed that each clone was
227 highly sensitive to the bacterial protein, with a half-maximal response at significantly lower
228 concentrations than for the synthetic peptides. No stimulation was observed in the absence of
229 allogeneic PBMC antigen presenting cells (APC), thus excluding stimulation from LPS/endotoxin
230 activity in the PFSGDS preparation (data not shown). This data suggests that a sub-population of
231 CeD associated T cells are potently activated by a bacterial protein contained in particular *P.*
232 *fluorescens* strains.

233

234 **Gluten challenge triggers response to bacterial mimic reactive T cells in CeD patients**

235 During a gluten free diet, the frequency of circulating, gliadin reactive T cells is typically very low
236 in CeD patients' blood and increases within days of gluten consumption. Oral gluten challenge
237 therefore provides a readout of a circulating, polyclonal memory-recall T cell response to gluten
238 that is disease specific²⁴. Hence, we used IFN- γ ELISpot assays to measure the reactivity of gluten-
239 specific T cells in the blood of 5 CeD patients to mimic peptides and PFSGDS before (day 0) and
240 on day 6 after a 3-day wheat gluten challenge to the mimic peptides and PFSGDS protein. ELISpot
241 assays were set up with a concentration range of 10-200 μ g/ml of the mimic peptides and 100-1000
242 μ g/ml PFSGDS (**Figure 4**). On day 6 after gluten challenge, the two gliadin peptides encompassing
243 overlapping epitopes DQ2.5-glia- α 1a/ α 2 and DQ2.5-glia- ω 1/ ω 2 (50 μ g/ml), used as positive
244 controls, led to significant responses in all 5 patients, whereas significant responses to 50 μ g/ml of
245 the mimic peptides *DQ2.5-P.fluor- α 1/ α 2a-15mer*, *DQ2.5-P.fluor- α 1/ α 2b-15mer*, *DQ2.5-P.aerug-*

246 *α2a-13mer* and DQ2.5-*B.copro-α2.2-13mer* showed a somewhat lower penetrance of 2/5, 1/5, 2/5
247 and 2/5 patients (**Figure 4a-d**), respectively, and 100 µg/ml PFSGDS induced significant responses
248 in the same patients (#670 and #496) as the peptide DQ2.5-*P.fluor-α1a-15mer* (**Figure 4e**), which
249 is encompassed by PFSGDS. Notably, the patient (#670) showed the strongest ELISpot responses
250 to the canonical gliadin peptides and to all bacterial peptides. As with the canonical gliadin
251 peptides, the T cell responses to the bacterial mimics and PFSGDS only reached significant levels
252 following gluten consumption, consistent with a gluten-specific recall response (**Figure 4f**). Thus,
253 our data shows that T cell responses to mimic peptides in patients' blood are induced by gluten
254 consumption and partially overlap with T cell responses to established gliadin epitopes.

255

256 **Differential TCR affinity towards deamidated gliadin and mimic epitopes**

257 LS2.8/3.15 and N12 TCR transduced T cell lines were more strongly activated by the bacterial
258 mimic peptide DQ2.5-*P.fluor-α1a* than by DQ2.5-glia-α1 (**Figure 2a, Supplementary Figure 1a**),
259 and the T cell lines JR5.1 and S16 differentially responded to the DQ2.5-glia-α2 mimics DQ2.5-
260 *P.aerug-α2a* and DQ2.5-*B.copro-α2a* (**Figure 2b, Supplementary Figure 1b**). To investigate the
261 basis for the differential activation by the bacterial mimic peptides, we expressed, refolded and
262 purified (i) the TCRs LS2.8/3.15, L6, JR5.1 and S16, and (ii) the peptide-HLA-DQ2 complexes
263 with the mimic peptides DQ2.5-*P.fluor-α1a*, DQ2.5-*P.fluor-α1b* and DQ2.5-*P.aerug-α2a*, and with
264 the corresponding DQ2.5-glia-α1 and DQ2.5-glia-α2 epitopes. We then performed surface plasmon
265 resonance (SPR) measurements to determine the affinities of the purified TCRs for these different
266 HLA-DQ2.5 complexes (**Figure 5**). The SPR measurements reflected the observations from the
267 peptide screening experiments, and indicated that the observed differences in T cell line activation
268 assays directly correlated with differences in binding affinities. The TCR LS2.8/3.15 bound to
269 HLA-DQ2.5-*P.fluor-α1a* with a significantly higher affinity (39.6 µM) than DQ2.5-glia-α1 and
270 HLA-DQ2.5-*P.fluor-α1b* (91.5 µM and >200 µM, respectively), while the L6 TCR had a clear
271 preference for HLA-DQ2.5-glia-α1 (21.4 µM) and only bound weakly to HLA-DQ2.5-*P.fluor-α1a*
272 (>200 µM), and showed no detectable binding to HLA-DQ2.5-*P.fluor-α1b* (**Figure 5a**). The results
273 with the HLA-DQ2.5-glia-α2 restricted TCRs JR5.1 and S16 similarly confirmed observations from
274 the T cell line stimulation assays, namely, JR5.1 bound to HLA-DQ2.5-glia-α2 and to HLA-DQ2.5-
275 *P.aerug-α2a* with similar affinities (83.7 µM and 132 µM, respectively), whereas the S16 TCR only
276 bound to HLA-DQ2.5-glia-α2 (13.5 µM), but not to HLA-DQ2.5-*P.aerug-α2a* (**Figure 5b**).
277 Accordingly, the affinity values of CeD TCRs towards bacterial mimics corresponded to that of
278 their stimulatory capacity.

279

280 **Bacterial ligand structural mimic of DQ2.5-glia-α1 epitope**

281 To establish how a bacterial mimic of the DQ2.5-glia- α 1 epitope was presented by HLA-DQ2.5, we
282 determined the crystal structure of the binary HLA-DQ2.5-*P.fluor- α 1a* complex to 1.9 Å resolution
283 (**Table 1**) and compared it to the structure of the HLA-DQ2.5-glia- α 1 complex. The HLA-DQ2.5-
284 *P.fluor- α 1a* structure aligned very well with the HLA-DQ2.5-glia- α 1 crystal structure, with a root
285 mean squared deviation (r.m.s.d) = 0.3Å for all C α atoms of the peptide binding cleft, and both
286 peptides were bound in a very similar conformation (**Figure 6a**). With the sequence variations
287 between the two peptides located in the p2 and p4 positions, the only notable difference in the
288 peptide was evident at the solvent exposed p2 position, where the p2-Met residue DQ2.5-*P.fluor- α 1a*
289 *alpha* was distinct from p2-Phe DQ2.5-glia- α 1. Nevertheless, the p4-Met residue in DQ2.5-*P.fluor- α 1a*
290 *alpha* was, despite its different chemical properties, almost perfectly aligned with p4-Gln in DQ2.5-
291 glia- α 1 (**Figure 6a**). Accordingly, the DQ2.5-*P.fluor- α 1a* epitope was a close structural mimic of
292 the DQ2.5-glia- α 1 epitope.

293

294 **Structure of the TCR-HLA-DQ2.5-*P.fluor- α 1a* complex**

295 To establish the molecular basis for how a HLA-DQ2.5-glia- α 1 reactive TCR could recognise the
296 bacterial mimic DQ2.5-*P.fluor- α 1a*, we determined the crystal structure of the LS2.8/3.15 TCR-
297 HLA-DQ2.5-*P.fluor- α 1a* complex to 2.8 Å resolution (**Table 1, Figure 6b-f**). The TCR docked on
298 HLA-DQ2.5-*P.fluor- α 1a* in a conventional orientation (**Figure 6b**), with an overall buried surface
299 area (BSA) of 2200 Å². The footprint of the LS2.8/315 TCR on HLA-DQ2.5-*P.fluor- α 1a* was
300 dominated by the CDR3 β loop, which contributed 37% of the BSA, and the remainder of the
301 interface was made up of smaller contributions by the remaining CDR loops and both α - and β -
302 framework residues (**Figure 6b**). The number of interactions the LS2.8/3.15 TCR made with the
303 pHLA were markedly skewed towards the HLA β -chain, which was reflected by the large BSA
304 contribution of 54.1% made by the HLA β -chain compared to 28.8% and 17.7% by the HLA α -
305 chain and peptide, respectively. Despite distinct CDR3 sequences and TRAV/TRBV usage, the
306 LS2.8/315 TCR revealed some degree of resemblance to that of the S2 TCR-HLA-DQ2.5-glia- α 1
307 complex¹⁴ in that the S2 TCR had an overall similar layout of CDR loops and covered a comparable
308 area on the pHLA with a nearly identical BSA of 2200 Å² and a large BSA contribution (54.8%) of
309 the HLA β -chain.

310

311 Both CDR3 α and CDR3 β loops of LS2.8/3.15 traversed the peptide binding cleft and interacted
312 with the HLA α - and β -chains (**Figure 6c**). Whilst the comparatively short CDR3 α loop made
313 limited contacts to Phe58 α and to Arg77 β of HLA-DQ2.5, the longer CDR3 β loop adopted a brace-
314 like conformation atop the central portion of the antigen-binding cleft. The interface with the HLA
315 α -chain was formed by Gln111 β at the tip of CDR3 β loop, which was wedged between the

316 sidechains of Phe58 α , Thr61 α and Asn62 α of the HLA α -chain helix, and formed H-bonds to
317 Asn62 α and the backbone of Phe58 α (**Figure 6d**). These interactions were further enhanced by the
318 adjacent β -framework residue Arg66 β , which formed vdw interactions with HLA residues Gln57 α ,
319 Phe58 α and Thr61 α (**Figure 6e**). On the opposing side of the peptide, the CDR3 β loop formed an
320 extensive vdw interface with the ridge of the HLA β -chain, involving residues Tyr60 β , Gln64 β ,
321 Asp66 β , Ile67 β and Arg70 β (**Figure 6d**). Moreover, this interface was further extended to Glu69 β ,
322 Ala73 β and Arg77 β through vdw interactions with CDR1 α and CDR2 α loops and a salt bridge
323 with the TCR α -chain framework residue Lys66 (**Figure 6f**).

324

325 The contacts between the LS2.8/315 TCR and the DQ2.5-*P.fluor- α 1a* peptide were exclusively
326 mediated through vdw interactions with hydrophobic peptide sidechains in p3-Pro, p5-Pro, p7-Leu
327 and p8-Pro (**Figure 6c**). Here, Ser110 α from the CDR3 α loop interacted with p3-Pro, and the
328 CDR3 β residues Glu109 β , Gln111 β and Ala113 β formed a larger contact area involving p5-Pro,
329 p7-Leu and p8-Pro. Moreover, p8-Pro interacted with Lys37 β and Tyr57 β from the CDR1 β and
330 CDR2 β loops, respectively. Accordingly, the LS2.8/315 TCR did not contact the P2 and P4
331 positions of the bacterial DQ2.5-*P.fluor- α 1a* mimic that differed from the DQ2.5-glia- α 1 epitope.
332 Thus, cross-reactivity was associated with the TCR seeing the similarities between the bacterial and
333 gliadin epitopes.

334

335 **Molecular mimicry drives TCR cross-reactivity.**

336 To establish the molecular basis for TCR recognition of the DQ2.5-glia- α 2 bacterial mimic, we
337 determined the structure of the JR5.1 TCR-HLA-DQ2.5-*P.aeru- α 2a* complex at 2.8Å resolution
338 (**Table 1, Figure 7**) and compared this to the JR5.1 TCR-HLA-DQ2.5-glia- α 2 complex structure¹⁴
339 (**Figure 7**). The overall structure of the JR5.1 HLA-DQ2.5-*P.aeru- α 2a* complex was very similar to
340 that of the corresponding HLA-DQ2.5-glia- α 2 complex, with only a slight tilt (2-3°) in the long axis
341 of the TCR towards the peptide N-terminus (**Figure 7a**) and an overlay of the peptides DQ2.5-
342 *P.aeru- α 2a* and HLA-DQ2.5-glia- α 2 only revealed very minor positional variations ($C\alpha$ r.m.s.d. =
343 0.17Å) (**Figure 7b**). Accordingly, the footprints of the JR5.1 TCR on HLA-DQ2.5-*P.aeru- α 2a*
344 (**Figure 7c**) and HLA-DQ2.5-glia- α 2 (**Figure 7d**), and) show the interactions with the DQ2.5-
345 *P.aeru- α 2a* peptide (**Figure 7e**) and the DQ2.5-glia- α 2 peptide (**Figure 7f**) were very similar. The
346 interactions between the HLA and the JR5.1 TCR CDR3 loops (**Supplementary Figure 4a**), and
347 the germline-encoded residues (**Supplementary Figure 4b and 4c**) were essentially conserved
348 between both complexes. Being slightly tilted towards the peptide N-terminus in the HLA-DQ2.5-
349 *P.aeru- α 2a* complex, the JR5.1 TCR formed additional interactions with the peptide N-terminal

350 side and lost some interactions on the C-terminal side of the peptide. Additional interactions in the
351 HLA-DQ2.5-*P.aeru-a2a* complex were a vdw-contact between Asn36 α and p2-Gln of the peptide
352 (**Figure 7e**) and two H-bonds between the backbone of the TRBV-framework residue Asp67 β and
353 the HLA α -chain residues Lys39 α and Gln57 α (**Supplementary Figure 4b**). Interactions lost in
354 the JR5.1 TCR-HLA-DQ2.5-*P.aeru-a2a* complex were located near the C-terminus of the peptide,
355 where CDR3 β Phe108 was lifted upwards by 1Å and thereby lost some of the vdw interactions with
356 the HLA β -chain (**Supplementary Figure 4a**). These subtle differences in binding were consistent
357 with the angular shift in TCR docking. Accordingly, molecular mimicry drives the TCR cross
358 reactivity across the gliadin and bacterial epitope.

359

360 **Discussion**

361 The *HLA II locus* is strongly associated with a number of T cell mediated autoimmune disorders,
362 where various mechanisms have been implicated². For example, in CeD, deamidation of gluten
363 peptides enables binding to HLA-DQ2/DQ8 molecules, thereby facilitating an acquired, aberrant
364 CD4⁺ T cell response. Nevertheless, the lack of penetrance of a given *HLA allele* to cause disease
365 indicates that other factors, including genetic and environmental, play a role in precipitating the
366 disease. The nature of the triggers and drivers relating to HLA-associated IMIDs remains unclear.

367

368 Population studies have implicated a range of environmental factors associated with CeD risk.
369 These include infections, particularly gastrointestinal infections, gluten feeding practices,
370 medications and perinatal factors such as season of birth¹⁹. An emerging concept is that these
371 environmental factors contribute to the disruption of oral tolerance²⁵. Specific viral infections
372 linked to CeD include rotavirus²⁶, adenovirus^{20,21}, reovirus²⁷ and enterovirus²⁸. However, as the
373 majority of CeD patients in these studies did not have evidence of prior viral exposure, other
374 triggers for CeD development are likely. A range of studies now support a secondary role for
375 opportunistic bacterial pathogens in CeD^{18,29-37}. Proteases from commensal gut bacteria are capable
376 of degrading gluten proteins and releasing immunogenic peptide fragments more amenable to
377 absorption, and can directly exacerbate gluten immunopathology in a HLA-DQ8 mouse model^{36,37}.
378 *P. fluorescens* is a minor component of the gut microbiota in humans, a rare cause of blood-borne
379 infection in humans³⁸⁻⁴⁰, and IgA antibodies to *P.fluorescens* are associated with Crohn's disease
380^{41,42}. In CeD, positive anti-*P.fluorescens* serology was observed in 86% of patients versus 31% of
381 healthy controls²⁹. Interestingly, sero-reactivity to microbial markers such as *Pseudomonas*
382 *fluorescens*-associated sequence I2 is seen in early CeD¹⁸ as well as CeD poorly responsive to a
383 gluten-free diet³⁴. This finding raises the possibility that immunoreactivity to microbial antigens

384 may play a role in CeD development or perpetuation of mucosal inflammation in patients avoiding
385 gluten.

386

387 There are several, potentially synergistic, mechanisms by which microbes are postulated to
388 contribute to the loss of T cell tolerance to gluten. Molecular mimicry, whereby T cells target
389 microbial antigens that mimic particular (self-)antigens associated with autoimmune disease,
390 provides a model for the initial phase of (self-)antigen sensitisation via cross-reactive T cells. This
391 mechanism was proposed in CeD based on sequence homology between adenovirus and gliadin but
392 this has never been substantiated^{20,21}. Our findings provide evidence that molecular mimicry to an
393 exogenous bacterial antigen may be a plausible primary mechanism contributing to the abrupt onset
394 of disease in HLA-DQ2⁺ individuals, usually in infancy, by inducing cross-reactive gluten-specific
395 CD4⁺ T cells. Colonisation of the intestinal mucosa by *P. fluorescens* may also be a potential
396 explanation for persistent mucosal injury in CeD patients strictly avoiding dietary gluten. We have
397 identified peptide mimics expressed in a range of related bacterial species. For example, DQ2.5-
398 *P.aeru-α2a* is present in several *Pseudomonas* and *Bordetella* species. Our findings support the data
399 that *P. aeruginosa* can modulate CeD inflammation and provides another mechanism distinct to the
400 effects of *P. aeruginosa* elastase^{36,37}. Accordingly, our data demonstrates that the prerequisites
401 exist for involvement of bacterial mimic peptides in the triggering of gluten-specific CD4⁺ T cells
402 from CeD patients, but more data is required in order to causally link specific bacteria to CeD
403 aetiology.

404

405 TCR recognition is highly degenerate and the sequence differences between canonical peptides and
406 molecular mimic peptides can, in principle, be quite substantial. Nevertheless, we used an approach
407 of a combined sequence homology search of microbes commonly associated with infections, the
408 human microbiota, or reported to be in association with CeD with structural and functional data on
409 CeD associated T cells. We identified peptides from common commensal and pathogenic bacteria
410 that cross-reacted with CeD patient-derived T cells restricted to the immunodominant gliadin
411 epitopes DQ2.5-glia-α1 and DQ2.5-glia-α2. Our structural and functional data identified that
412 molecular mimicry was the underlying molecular mechanism for T cell cross-reactivity. To date,
413 there are only a few examples of candidate mimic epitopes in IMID that have been identified^{43 44}
414⁴⁵. Our study exemplifies how mimic epitopes can be identified using both homology and reactivity
415 of disease associated T cells, and demonstrates that common and abundant bacteria do express
416 highly active mimic antigens that closely resemble two immunodominant and deamidated epitopes
417 targeted by pathogenic T cells in CeD.

418

419 Thus, our study highlights the possibility that CeD results from the triggering of a host T cell
420 response to bacteria that cross-reacts with gluten epitopes. Once initiated this may be followed by
421 gluten driven expansion of the cross-reactive T cell receptor repertoire and epitope spreading. This
422 may explain why only a minority of the gluten-specific T cell response induced by oral gluten
423 challenge responds to the bacterial mimic epitopes. Finally, the high frequency of mimic peptides
424 in our sample set of candidate peptides suggests that bacteria likely contain a pool of mimic
425 antigens that fit into the context of other autoimmune diseases. Ultimately, such knowledge may be
426 used to prevent IMIDs in genetically predisposed individuals.

427

428 **Acknowledgements**

429 We thank the staff at the Australian Synchrotron for assistance with data collection, the staff at the
430 Monash Macromolecular crystallization facility. We thank the CeD volunteers who participated in
431 this study. This work was supported by a program grant from the National Health and Medical
432 Research Council of Australia (NHMRC) and the Australian Research Council (ARC)
433 (CE140100011). FK is supported by the collaboration project TIMID (LSHM18057-SGF) financed
434 by the PPP allowance made available by Top Sector Life Sciences & Health to Samenwerkende
435 Gezondheidsfondsen (SGF) to stimulate public-private partnerships and co-financing by health
436 foundations that are part of the SGF. AWP is supported by an NHMRC Principal Research
437 Fellowship; JR is supported by an Australian ARC Laureate Fellowship.

438

439 **Competing interests Declaration**

440 RPA is an employee of ImmusanT, Inc., a company developing a celiac disease immunotherapy.
441 RPA and JAT-D are inventors of patents, owned or licensed by ImmusanT, Inc., relating to the
442 diagnostic application of gluten challenge, and utilisation of gluten-derived T cell epitopes for use
443 in therapeutics.

444

445

446

447 **Figure legends**

448

449 **Figure. 1: Identification of microbial mimic peptides for CeD epitopes using TCR structural**
450 **and functional data.** (a) Location of TCR – peptide interactions in published TCR-pHLA
451 structures and TCR sensitivity to individual peptide substitutions in HLA-DQ2.5-glia- α 1, HLA-
452 DQ2.5-glia- ω 1 and HLA-DQ2.5-glia- α 2. Peptide surface representations from TCR-pHLA
453 structures are coloured according to contacting CDR loop (red: CDR1 α , cyan: CDR3 α , orange:
454 CDR1 β , purple: CDR2 β , blue: CDR3 β). TCR sensitivity to Ala mutation is expressed (blue bars) as
455 fraction of TCRs that loose >75% function upon Ala substitution in p1-p9 of the peptide. (b)
456 Selected mimic peptides with negative charge at canonical deamidation site and substitution score
457 based on TCR sensitivity.

458

459 **Figure. 2: Bacterial mimic peptides and parent protein potently stimulate CeD patient**
460 **derived T cells.** Screening of bacterial mimic peptides for activation of TCR transduced of SKW3
461 TCCs. CD69 and CD3 expression levels of (a) DQ2.5-glia- α 1 restricted TCCs and (b) DQ2.5-glia-
462 α 2 restricted TCCs were measured after 16h incubation the presence HLA-DQ2⁺ BLCLs and 32
463 μ g/ml peptide or 500 μ g/ml PFSGDS protein. The percentage of CD69^{high} and CD3^{low} TCCs (mean
464 \pm standard deviation (SD) from 2 independent experiments with 2 replicates) was used as a relative
465 indicator of T cell activation. Responses were considered positive where the mean %CD69^{high}
466 signal exceeded background (DMSO) plus 2 times SD, and significant, where CD69^{high} was more
467 than 3 SD above background.

468

469 **Figure. 3: HLA-DQ2⁺ antigen presenting cells process PFSGDS and present antigenic mimic**
470 **peptide, and patient derived T cells proliferate in response to bacterial mimic peptides or**
471 **PFSGDS protein.** Peptides derived from succinylglutamate desuccinylase were identified
472 following antigen feeding of HLA-DQ2.5+ or HLA-DQ8+ cells and subsequent elution of HLA-
473 DQ-bound peptides and sequencing by LC-MS/MS. (a) Position 261-299 of succinylglutamate
474 desuccinylase reveals disparity of nested peptide presentation between DQ2- and DQ8-expressing
475 cells. Region in bold indicates peptide with highest confidence identification score. (b) b-, y- and
476 internal-fragment ion assignments for peptide GEPmPmPELPYPATP (lowercase m denotes
477 oxidised methionine) eluted from 9022 (DQ2+) cells. (c, d) Proliferation of CeD patient derived T
478 cell lines induced by mimic peptides and PFSGDS protein. (c) Proliferation of DQ2.5-glia- α 1
479 restricted and DQ2.5-glia- α 2 restricted T cell lines (left and right of dashed line, respectively) (d)
480 Proliferation of patient derived DQ2.5-glia- α 1 restricted T cell lines induced by dilutions of mimic
481 peptides and PFSGDS protein. In total 19 independent T cell clones were tested against gliadin and

482 mimic peptide epitopes in 18 experiments. One T cell clone was tested 5 times, 4 were tested 4
483 times, 9 were tested 3 times, 3 were tested twice, 2 were tested once. In 9 independent experiments
484 the response to the bacterial PFSGDS protein was determined as well. In 5 of those experiments the
485 T cell clones were tested against a concentration range of the PFSGDS protein. Representative
486 results are shown.

487

488 **Figure. 4: T cell cross-reactivity following gluten challenge.** IFN- γ ELISpot assays show
489 significant T cell reactivity to mimic peptides and PFSGDS protein in PBMCs from five CeD
490 patients after wheat gluten challenge. T cell activation (spot-forming units; SFU/10⁶ PBMCs) was
491 measured in the presence of varying concentrations of the mimic peptides: (a) DQ2.5-P.fluor- α 1/2a-
492 15mer, (b) DQ2.5-P.fluor- α 1/2b-15mer, (c) DQ2.5-P.aerug- α 2a-13mer, (d) DQ2.5-B.copro- α 2.2-
493 13mer, and (e) PF SGDS protein; μ g/mL concentrations shown on each graph. T cell responses
494 against 50 μ g/mL control gliadin peptides (containing DQ2.5-glia- α 1a/ α 2 and DQ2.5-glia- ω 1/ ω 2)
495 are shown on each graph as a comparison. Mean \pm SD of duplicate wells are shown. * Responses
496 above the cut-off are considered positive. (f) T cell responses against 100 μ g/mL bacterial peptide,
497 250 μ g/mL protein, or 50 μ g/mL control gliadin peptides in all patients prior to (day 0) and day 6
498 after gluten challenge in the same five CeD patients. Response cut-offs are depicted as dotted lines.

499

500 **Figure. 5: Surface plasmon resonance affinity measurements.** (a) Binding affinities of DQ2.5-
501 glia- α 1 restricted TCRs LS3.15 and L6 were determined for surface bound HLA-DQ2.5-glia- α 1,
502 HLA- DQ2.5-P.fluor- α 1a, and HLA-DQ2.5-P.fluor- α 1b. (b) Binding affinities of DQ2.5-glia- α 2
503 restricted TCRs JR5.1 and S16 were determined for surface bound HLA-DQ2.5-glia- α 2 and HLA-
504 DQ2.5-P.aerug- α 2a.

505

506 **Figure. 6: Structural basis for the recognition of HLA-DQ2.5-P.fluor- α 1a** (a) Overlay of the
507 crystal structures of the binary complexes HLA-DQ2.5-P.fluor- α 1a (purple sticks) and HLA-
508 DQ2.5-glia- α 1 (grey sticks) shows good alignment for the peptides. b-f) Crystal structure of the
509 LS2.8/3.15 TCR - HLA-DQ2.5-P.fluor- α 1a ternary complex. Colours: CDR loops and
510 corresponding TCR footprint contacts are coloured red, pink, cyan, orange, purple and blue for
511 CDR1 α , CDR2 α , CDR3 α , CDR1 β , CDR2 β , CDR3 β , respectively, and framework residues are
512 coloured green. The peptide and HLA α - and β -chains are coloured grey, light green, and light
513 yellow, respectively. (b) TCR docking angle, footprint and BSA contributions. (c) Interactions
514 between the LS2.8/3.15 TCR and the DQ2.5-P.fluor- α 1a peptide. (d) Interactions between the
515 CDR3 region of LS2.8/3.15 and the HLA. (e) Germline encoded interactions between LS2.8/3.15
516 and the HLA α -chain. (f) Germline encoded interactions between LS2.8/3.15 and the HLA β -chain.

517

518 **Figure. 7: Molecular mimicry drives cross-recognition of bacterial epitope HLA-DQ2.5-**
519 ***P.aerug-a2a*.** Comparison of the ternary complexes between the JR5.1 TCR and HLA-DQ2.5 with
520 bound peptides HLA-DQ2.5-*P.aerug-a2a* and HLA-DQ2.5-*glia-a2*. Colours: CDR loops and
521 corresponding TCR footprint contacts are coloured red, pink, cyan, orange, purple and blue for
522 CDR1 α , CDR2 α , CDR3 α , CDR1 β , CDR2 β , CDR3 β , respectively, and framework residues are
523 coloured green. The peptide and HLA α - and β -chains are coloured grey, light green, and light
524 yellow, respectively. (a) Overlay of the ternary complex structures of the JR5.1 TCR with HLA-
525 DQ2.5-*P.aerug-a2a* and HLA-DQ2.5-*glia-a2* shows a small tilt in the angle in which the JR5.1
526 TCR binds to HLA-DQ2.5-*P.aerug-a2a* and HLA-DQ2.5-*glia-a2*. (b) Overlay of the peptides
527 HLA-DQ2.5-*P.aerug-a2a* (grey sticks) and HLA- DQ2.5-*glia-a2* (beige sticks) in the respective
528 ternary complexes. (c, d) footprint and docking angle and BSA contributions of the JR5.1 TCR
529 binding to c) HLA-DQ2.5-*P.aerug-a2a* and d) HLA-DQ2.5-*glia-a2*. (e, f) Comparison of the
530 interface between the JR5.1 TCR and the peptides (e) DQ2.5-*P.aerug-a2a* and (f) HLA-DQ2.5-
531 *glia-a2*.

532

533 **Methods**

534

535 **Protein expression and purification**

536 HLA-DQ complexes. The extracellular domains of HLA-DQ2.5 (HLA-DQA1*5:01 and HLA-
537 DQB1*02:01) with the canonical gliadin epitopes and the HLA-DQ8-CLIP complex were produced
538 as previously described^{13,14}. For the bacterial epitopes the peptides DQ2-*P.fluor-a1a*:
539 APMPMPPELPYP, DQ2-*P.fluor-a1b*: APMPLPDLPYP, and DQ2-*P.aeru-a2a*: AMVVQSELPYPE
540 were covalently linked to the N-terminus of the HLA-DQ2.5 β -chain using the linker sequence
541 GSGGSIEGRGGSG. HLA-DQ complexes expressed in the supernatant of baculovirus infected in
542 Hi5 insect cells were concentrated and diafiltrated into 10 mM Tris, pH 8, and 500 mM NaCl using
543 a Cogent M1 TFF system (Merck Millipore) and subsequently purified via immobilised metal
544 affinity (Ni Sepharose 6 Fast Flow; GE Healthcare), size exclusion (Superdex 200; GE Healthcare)
545 and anion-exchange (HitrapQ; GE Healthcare) chromatography. Prior to crystallisation
546 experiments, the C-terminal domains of the constructs were removed by cleavage with Enterokinase
547 (New England Biolabs) followed by a second round of anion-exchange chromatography.

548

549 T cell receptors. The extracellular domains of the TCR α and β chains with an engineered interchain
550 disulfide bond were expressed in E coli and refolded and purified as described previously¹³.

551

552 PFSGDS. *E. coli* BL21-DE3 transformed with a pET30 vector containing the *E. coli* codon
553 optimised DNA sequence of PFSGDS in frame with a C-terminal His6-Tag was grown in LB media
554 at 37 ° C to OD₆₀₀ =0.7 and induced with 500µM IPTG for 4 h at 25° C. Harvested cells were
555 resuspended in ice cold 20 mM Tris pH8.0, 300mM NaCl, 0.5 mM tris(2-carboxyethyl)phosphine
556 (TCEP) and 0.2 mM PMSF, and lysed by sonication. The lysate was cleared by centrifugation for
557 30 min at 25000 g, supplemented with 20mM Imidazole and passed over Ni-Sepharose. To remove
558 contaminants and bacterial lipids, bound PFSGDS was extensively washed using 8 column volumes
559 (CV) of buffer A (20 mM Tris pH8.0, 300mM NaCl, 20mM Imidazole, 0.2 mM TCEP), followed
560 by 40 CV of buffer B (20 mM Tris pH8.0, 300mM NaCl, 0.2 mM TCEP, 0.1% Triton X100) and
561 again 8 CV of buffer A. After elution with 300 mM Imidazole in buffer A, the protein was further
562 purified via size exclusion chromatography (Superdex 200; GE Healthcare) in PBS.

563

564 **Surface plasmon resonance**

565 Surface plasmon resonance measurements were performed on a BIACORE 3000 instrument
566 essentially as described previously¹⁴. Briefly, purified HLA-DQ2 complexes and HLA-DQ8-clip as
567 background control were biotinylated and immobilised using a Biotin Capture Kit (GE healthcare,
568 Parramatta, Australia) to a surface loading of 900-1500 response units. Serial dilutions of purified
569 TCRs in SPR buffer containing (20mM HEPES pH7.4, 150 mM NaCl, 2 mM EDTA, 0.005%
570 surfactant P20) were passed over the chip at a flow rate of 10 µL/min for 90s. two Two
571 independent experiments with two replicates were performed for each TCR and equilibrium
572 dissociation constants were determined by fitting a single site binding model to the data.

573

574 **Crystallisation, diffraction data collection and structure determination**

575 Crystals were grown at 20°C via the hanging drop vapor diffusion method using equal volumes of
576 protein (7-10 mg/ml in 10mM Tris-HCl pH 8.0, 150 mM NaCl) and crystallisation solutions. HLA-
577 *DQ2-P.fluor-α1a* was crystallised with 18% PEG3350 and 0.15M NH₄H₂PO₄; the ternary complex
578 LS2.8/3.15 – HLA-DQ2.5P.fluor-α1a with 22% PEG3350, 0.2M Na-K Tartrate, 0.08 M MES
579 pH6.5; and the the ternary complex JR5.1 – HLA-*DQ2-P.aerug-α2a* in 23%PEG3350, 0.01mM Na-
580 Acetate, 0.1 M Tris pH8.0. Prior to data collection crystals of HLA-*DQ2-P.fluor-α1a* and the two
581 ternary complexes were cryoprotected in reservoir solution supplemented with 18 % glycerol or
582 20% PEG 400, respectively, and frozen in liquid N₂. X-ray diffraction data was collected at the
583 Australian Synchrotron using the MX1 beamline for HLA-*DQ2-P.fluor-α1a* and LS2.8/3.15 - HLA-
584 *DQ2-P.fluor-α1a*, and at the MX2 beamline for JR5.1 - HLA-*DQ2-P.aeru-α2a*. Crystals were
585 exposed at 100K using a single wavelength (0.953725 Å, 0.94640 Å and 0.95372 Å, respectively)
586 and the diffraction data was processed using XDS⁴⁶ and merged using Aimless of the CCP4

587 package⁴⁷. The structures were solved via molecular replacement in Phaser⁴⁸ using previously
588 published coordinates as search models; HLA-DQ2 (PDB code 6MFG)²², and TCRs T316 and
589 JR5.1 (PDB codes: 4Z7W and 4OZH)^{13,14} for the LS2.8/3.15 – HLA-DQ2.5P.fluor- α 1a and JR5.1
590 – HLA-DQ2-P.aerug- α 2a structures, respectively. Model building, refinement and validation was
591 carried out using Coot⁴⁹ and the Phenix software package⁵⁰. The geometries of the refined
592 structure models of were validated in Phenix, which indicated that HLA-DQ2-P.fluor- α 1a,
593 LS2.8/3.15 – HLA-DQ2.5P.fluor- α 1a JR5.1 – HLA-DQ2-P.aerug- α 2a contained 0%, 0.12% and
594 0.069% of Ramachandran outliers, respectively. The structure factors and refined atomic models
595 were deposited in the PDB databank (PDB codes 6U3M, 6U3N, 6U3O).

596

597 **Cell lines**

598 SKW3 cells and TCR transduced SKW3 cell lines were maintained in RPMI-1640 supplemented
599 with 50 IU/ml penicillin, 50 μ g/ml streptomycin, 2mM Glutamine, 1x non-essential aminoacids, 1
600 mM Pyruvate, 10mM HEPES and 10% FBS (RF10⁺ media); EBV-transformed B-lymphoblastoid
601 cell lines 9022 (COX, DQ2⁺; DQA1*05:01, DQB1*02:01) and 9033 (BM14, DQ8⁺; DQA1*03,
602 DQB1*0302) were maintained in the same media containing 15% FBS (RF15⁺ media); Prior to
603 SKW3 T cell stimulation and antigen feeding experiments all cells were rested for 24 h in fresh RF⁺
604 media supplemented with 10% FCS, and cell density was adjusted to 2*10⁶ cells/ml. The B cell
605 hybridomas SPV-L3 (anti-HLA-DQ), L243 (anti-HLA-DR) and b7/21 (anti-HLA-DP) were grown
606 in RPMI-1640 supplemented with 5% FBS. TCR transduced cell lines SKW3.LS2.8/3.15,
607 SKW3.L6, SKW3.N12, SKW3.JR5.1 and SKW3.S16 were produced via retroviral transduction of
608 the $\alpha\beta$ TCR-deficient T cell leukemia cell line SKW-3, as previously described⁵¹.

609

610 **T cell proliferation assays**

611 Proliferation assays were performed in triplicate in 150 μ l Iscove's modified Dulbecco's medium
612 supplemented with glutamine (Gibco) and 10% human serum in 96-well flat-bottom plates. Briefly,
613 antigen-presenting cells (APCs) were loaded with antigen for 2 h, after which 20,000 gluten-
614 specific T cells were added. As APCs we used 100.000 irradiated HLA-DQ2.5-matched allogeneic
615 PBMCs (3,000 rad). Synthetic peptides were used at a final concentration of 6 μ g/ml. After 48 h at
616 37 °C, cultures were pulsed with 0.5 μ Ci of 3H-thymidine and harvested 18 h later. As positive
617 controls 13-mer versions of the DQ2.5-glia- α 1 (LQPFPPQPELPYPQ) and DQ2.5-glia- α 2
618 (PFPQPEPLYPQPQ) epitopes were used.

619

620 **SKW3 T cell stimulation assays**

621 T cell stimulation assays monitoring CD69 and CD3 expression of SKW3.TCR cells were
622 conducted in 96-well round bottom tissue culture plates: Serial dilutions of peptides (10mg/ml in
623 DMSO), PFSGDS protein (34 mg/mL in PBS) or DMSO were set up in 50 μ l media at room
624 temperature, followed by addition of 2×10^5 antigen presenting cells (9022 or 9033 BLCLs) and 10^5
625 SKW3.TCR cells (LS2.8/3.15, L6, N12, JR5.1 or S16) to a final volume of 200 μ l/well. For
626 antibody controls, antigen presenting cells were supplemented with blocking antibodies SPV-L3,
627 L243 or b7/21 (5 μ g/well) prior to addition to the wells. Cells were incubated for 16 h (37° C, 5%
628 CO₂) and subsequently washed with cold PBS and stained with Zombie Aqua™ viability dye (BD
629 Pharmingen) followed by phycoerythrin-conjugated mouse anti-human CD69 (FN50; BD
630 Pharmingen) and allophycocyanin-conjugated mouse anti-human CD3 (OKT3; BD Pharmingen).
631 Cells were subsequently fixed with 2% Formaldehyde and stored in the dark at 4° C for up to 36 h
632 prior to analysis. To determine surface expression levels of CD3 and CD69, the cells were analysed
633 on a LSRFortessa™ X-20 instrument (BD-Biosciences) (refer to **Supplementary Figure 5** for
634 gating strategy). Data were analysed using FlowJo 7.6 (Tree Star, OR, USA) and plotted in Prism
635 (GraphPad San Diego, CA).

636

637 **Antigen feeding and mass spectrometry**

638 300×10^8 antigen presenting cells (9022 and 9033 BLCLs) were incubated for 16 h at 37° C in the
639 presence of 300 μ g/mL purified PFSGDS and subsequently harvested by centrifugation at 350g.
640 After washing thrice with ice cold PBS, cell pellets were frozen in liquid N₂ and stored at -80° C.
641 Peptides presented by HLA-DQ were isolated via immunoprecipitation and analysed via as
642 spectrometry as follows: Cell pellets were ground using a Retsch mixer mill (MM400) and lysed in
643 0.5% (v/v) NP-40, 50 mM Tris pH 8.0, 150 mM NaCl, and protease inhibitor cocktail (Roche
644 cOmplete Protease Inhibitor) and HLA-DQ-peptide complexes isolated by immunoaffinity
645 purification using protein A-crosslinked anti-DQ antibody (10mg per sample, clone SPV-L3).
646 HLA-peptide complexes were dissociated by addition of 10% (v/v) acetic acid and peptides
647 separated from heavy chain by RP-HPLC fraction on an Äkta Ettan (GE Healthcare) system using a
648 Chromolith SpeedROD (RPC18 end-capped, 100 \times 4.6-mm) column (Merck), over an increasing
649 gradient mixture of buffer A (0.1% v/v trifluoroacetic acid (TFA) in water) and buffer B (80% v/v
650 acetonitrile, 0.1% v/v TFA in water). Fractions were pooled using a concatenating scheme of every
651 seventh fraction, dried down using a centrifugal concentrator (Labconco) and resuspended in 20 μ L
652 of mass spectrometry buffer A (0.1% v/v formic acid in water). Samples were analysed on a
653 TripleTOF® 6600 (SCIEX) mass spectrometer, equipped to an on-line Eksigent Ekspert nanoLC
654 415 system (SCIEX) using a trap column (ChromXP C18, 3 μ m 120 Å, 350 μ m \times 0.5 mm
655 (SCIEX)) maintained at an isocratic flow of buffer A (2% v/v acetonitrile, 0.1% v/v formic acid in

656 water) at 5 μ L/min for 10 min. Peptides were separated across an analytical column (ChromXP
657 C18, 3 μ m 120 \AA , 75 μ m \times 15 cm (SCIEX)) by increasing linear concentrations of buffer B (80%
658 v/v acetonitrile, 0.1% v/v formic acid in water) at a flow rate of 300 nL/min for 75 min. Up to 20
659 MS/MS spectra were acquired per cycle using an information dependent acquisition strategy with
660 accumulation times of 200 ms and 150 ms for MS1 and MS2, respectively. MS1 scan range was set
661 to 300-1800 m/z and MS2 set to 80-2000 m/z. To prevent multiple sequencing of the same peptide,
662 MS1 masses were excluded for sequencing after two occurrences for 30 seconds. Data were
663 analysed using PEAKS Studio v8.5 (Bioinformatics Solutions Inc) with the following settings:
664 parent mass error tolerance of 50 ppm; fragment mass error tolerance of 0.1 Da; no enzyme
665 cleavage; variable modifications of deamidation (NQ), phosphorylation (STY), oxidation (M). Data
666 were searched against either the human proteome (Uniprot, November 2018) appended with the
667 sequence of PFSGDS, or against PFSGDS alone.

668

669 **Ex vivo stimulation of T cells from CeD patients after gluten challenge**

670 *Participants and gluten challenge*

671 The study was approved by the Human Research Ethics Committees of the Walter and Eliza Hall
672 Institute (no. 03/04) and the Royal Melbourne Hospital (no. 2003.009). CeD participants were
673 adults aged between 18-70 years, were diagnosed according to ESPGHAN criteria¹, and following a
674 gluten-free diet for at least 3 months prior to recruitment (**Supplementary table 1**). Whole blood
675 samples were collected prior to (day 0, D0) and 6 days (D6) following 3-day oral wheat gluten
676 challenge consisting of 4 slices of Bakers Delight white bread block loaf cut to toasting size
677 thickness each day for 3 days. Symptoms were recorded on days 1-6 using the CeDPRO². Baseline
678 D0 blood was sent for serological screening for tissue transglutaminase-IgA and deamidated gliadin
679 peptide-IgG levels at Melbourne Pathology.

680

681 **IFN- γ ELISpot Assay**

682 Peripheral blood mononuclear cells (PBMCs) from heparinized CeD patient whole blood were
683 isolated using Ficoll-Paque Plus density-gradient centrifugation (GE Healthcare, Buckinghamshire,
684 UK) within 4 hours of collection. Overnight IFN- γ ELISpot assays (Mabtech) were performed
685 following modified manufacturer's instructions. ELISpot plates (Millipore Cat. #MSIPS4510) were
686 coated with anti-human IFN- γ mAb (1- D1K;10 μ g/mL) overnight at 4 $^{\circ}$ C. Plates were washed in
687 PBS and blocked with 10% FCS in RPMI1640. Peptides were tested at a final concentration of 10-
688 200 μ g/mL and protein at 0.1-1 mg/mL added in a 25 μ L volume. PBMC were resuspended in
689 complete medium: composed of RPMI 1640, 1x GlutaMAX, 100 %M NEAA from Gibco Thermo
690 Fisher Scientific, 50 %M 2-ME (Sigma), 10% pooled human serum (Australian Red Cross Blood

691 Service), and $3-5 \times 10^5$ PBMC in 100 μ L were added per well. Control antigens tested included alpha
692 and omega wheat gliadin peptides containing the overlapping epitopes DQ2.5-glia- α 1a/ α 2 and
693 DQ2.5-glia- ω 1/ ω 2 (Figure 1a), 5 μ g/mL Tetanus toxoid (Enzo Life Sciences), and 2.5 μ g/mL
694 phytohemagglutinin-L (PHA-L; Sigma-Aldrich, St. Louis, MO). The following bacterial peptides
695 were screened: DQ2.5-P.fluor- α 1/2a-15mer, DQ2.5-P.fluor- α 1/2b-15mer, DQ2.5-P.aerug- α 2a-
696 13mer and DQ2.5-B.copro- α 2.2- 13mer (Figure 1b), as well as the PFSGDS protein. Following
697 overnight incubation, plates were washed with PBS/0.05% Tween 20 and PBS, and developed with
698 Mabtech anti-human IFN- γ secondary antibody (7-B6-1-Biotin; 1 μ g/mL), Streptavidin-ALP (Cat.
699 #3420-2A; 1:1000 in 0.5% FCS/PBS), and 0.45 μ M filtered Mabtech BCIP/NBT substrate (Cat.
700 #3650; 1:2 in distilled water). Spot-forming units (SFU) were counted using an automated ELISpot
701 reader (Autoimmun Diagnostika; Strassberg, Germany). Raw SFU were adjusted to SFU/ 10^6
702 PBMC to normalise between individuals. A cut-off of 20 SFU/ 10^6 PBMC was used to determine
703 positive responses, based on 5xSD calculated from the average of the 'No antigen' negative
704 controls from all patients. Mean of replicate wells and standard deviation measurements were
705 calculated and graphed using GraphPad prism version 7.0 (GraphPad, San Diego, CA).
706

707 **Table 1: Data collection and refinement statistics**
 708

	HLA-DQ2.5- <i>P.fluor-ala</i>	TCR LS2.8/3.15 - HLA-DQ2.5- <i>P.fluor-ala</i>	TCR JR5.1 - HLA-DQ2.5- <i>P.aeru-a2a</i>
Data collection			
Space group	P 21 21 21	C 2 2 21	P 1 21 1
Cell dimensions			
<i>a, b, c</i> (Å)	94.935 96.276 105.74	59.98 239.47 147.46	69.057 157.65 106.1
α, β, γ (°)	90 90 90	90 90 90	90 96.53 90
Resolution (Å)	47.47 - 1.9 (1.968 - 1.9)	46.48 - 2.8 (2.9 - 2.8)	47.03 - 2.743 (2.841 - 2.743)
R_{pim}	0.05776 (0.4427)	0.02771 (0.4184)	0.04437 (0.3744)
$I / \sigma I$	25.38 (2.16)	17.05 (1.85)	13.40 (2.00)
Completeness (%)	99.62 (96.94)	99.91 (99.92)	99.26 (98.60)
Redundancy	7.4 (7.5)	2.0 (2.0)	3.6 (3.4)
Refinement			
Resolution (Å)	47.47 - 1.9	46.48 - 2.8	47.03 - 2.743
No. reflections	76853 (7564)	26697 (2609)	58558 (5789)
$R_{\text{work}} / R_{\text{free}}$	0.1911 (0.2888) /0.2213 (0.3103)	0.2140 (0.3416) /0.2702 (0.3830)	0.2056 (0.3354) /0.2423 (0.3655)
No. atoms			
Protein	6008	6463	12766
Ligand/ion	99	14	56
Water	479	1	66
<i>B</i> -factors			
Protein	47.28	94.45	84.74
Ligand/ion	55.83	140.17	94.42
Water	45.65	60.47	56.02
R.m.s. deviations			
Bond lengths (Å)	0.007	0.004	0.002
Bond angles (°)	0.87	0.98	0.55

709 *Values in parentheses are for highest-resolution shell.
 710

711

712

713

714 **Supplementary data**

715

716 **Supplementary Figure Legends**

717 **Supplementary Figure. 1: Concentration dependent stimulation of SKW3 T cell clones with**

718 **mimic peptides.** Screening of bacterial mimic peptides for activation of TCR transduced of SKW3

719 TCC using different concentrations of peptide (0-32 $\mu\text{g/ml}$), or PFSGDS protein (0-500 $\mu\text{g/ml}$).

720 CD69 and CD3 expression levels of (a) DQ2.5-glia- α 1 restricted TCCs and (b) DQ2.5-glia- α 2

721 restricted TCCs were measured after 16 h incubation in the presence of the indicated antigen and

722 HLA-DQ2.5⁺ BLCLs. Data shown is percentage of cells with CD69^{high} or CD3^{low} (mean +/- SD

723 calculated as from two independent experiments with two replicates). Responses were considered

724 positive where CD69^{high} exceeded averaged background plus 2 times SD (<DMSO> + 2 SD), and

725 significant, where CD69^{high} was more than 3 SD above averaged background.

726

727 **Supplementary Figure. 2: Stimulation of SKW3 T cell clones with longer mimic peptides.** (a)

728 Screening of long bacterial mimic peptides (32 $\mu\text{g/ml}$) and PFSGDS (500 $\mu\text{g/ml}$) protein for

729 activation CD69 of HLA-DQ2.5-glia- α 1a and HLA-DQ2.5-glia- α 2 restricted TCR transduced

730 SKW3 TCC and specific blocking of stimulation by anti-HLA-DQ, but not anti-HLA-DR-, or anti-

731 HLA-DP antibodies. CD69 expression levels of TCR transduced SKW3 TCC were measured in

732 response to peptides or PFSGDS with HLA-DQ8⁺ or HLA-DQ2⁺ antigen presenting cells in the

733 presence of HLA blocking antibodies. Data shown is percentage of cells with CD69^{high} averaged

734 from two independent experiments with two technical replicates. Responses were considered

735 positive where CD69^{high} exceeded averaged background plus 2 times SD (<DMSO> + 2 SD). (b)

736 Sequences of long versions of active mimic peptides identified in initial screen.

737

738 **Supplementary Figure. 3: Expression and purification of PFSGDS protein.** SDS-PAGE gel of

739 purified PFSGDS protein suggests the protein is >95% pure.

740

741 **Supplementary Figure. 4: Minor structural differences in the JR5.1 TCR – HLA-DQ2.5**

742 **interface.** Comparison of the of the interactions between the JR5.1 TCR and the HLA-DQ2.5 in

743 the ternary complex with HLA-DQ2.5-*P.aerug*- α 2a (left) and HLA-DQ2.5-glia- α 2 (right). Colours:

744 CDR loops and corresponding TCR footprint contacts are coloured red, pink, cyan, orange, purple

745 and blue for CDR1 α , CDR2 α , CDR3 α , CDR1 β , CDR2 β , CDR3 β , respectively, and framework

746 residues are coloured green. The peptide and HLA α - and β -chains are coloured grey, light green,

747 and light yellow, respectively. (a) Comparison of interactions between the CDR3 region of the

748 JR5.1 TCR and the HLA. (b) Comparison of germline encoded interactions between the JR5.1 TCR

749 and the HLA α -chain. (c) Comparison of germline encoded interactions between the JR5.1 TCR and
750 the HLA β -chain.

751 **Supplementary Figure. 5: Gating strategy for T cell stimulation assays.** TCR transduced
752 SKW3 cells were gated as follows: Lymphocytes (FCS-A/SSC-H); single cells (FSC-A/FSC-H);
753 live cells (AQUA stain, BV525-A low); GFP expression (B530-A high). T cell activation was
754 measured via staining of CD69 and CD3 (PE-anti-CD69, YG585-A vs. APC-anti-CD3, R670-A)
755 and expressed as % of cells in the respective activation gate (CD69^{high} and CD3^{low}). Gates for T
756 cell activation were set for each TCR transduced SKW3 line to include 5-10 % of cells in the
757 vehicle control sample.

758

759

760

761

762 **Supplementary Table 1 – CeD cohort details for gluten challenges**

Challenge symptoms (+ mild; ++ moderate; +++ severe) ^c																	
Subject	Age	Sex	HLA-DQ ^a	tTG-IgA	DGP-IgG	3d ^b	P	Bl	C	D	F	S	N	V	H	L	Other
0670	61	F	DQ2.5/DQ8	17 (<20) ^d	44 (<20)	Y		+					+				
0041	68	F	DQ2.5/DQX	ND	ND	Y	+										
0148	63	M	DQ2.5/DQX	3 (<20)	<3 (<20)	Y	+++	+++		+++	+++	+++			+	+++	
0570	61	M	DQ2.5/DQX	4 (<20)	<3 (<20)	Y											Asymptomatic
0496	43	F	DQ2.5/DQX	ND	ND	Y	+	+			+		++		++	+++	

^a X denotes allele other than DQ2.5

^b 3d indicates subjects completing all 3 days of gluten challenge (Y = YES, N = NO)

^c N = nausea, Bl = bloating, V = vomiting, D = diarrhea, L = lethargy, P = pain/cramping, C = constipation, S = loose stool, F = flatulence, H = headaches

^d numbers in brackets indicate the serological assay detection cut-off. Red result indicates a positive result.

ND = not done

763

764 References

765

766

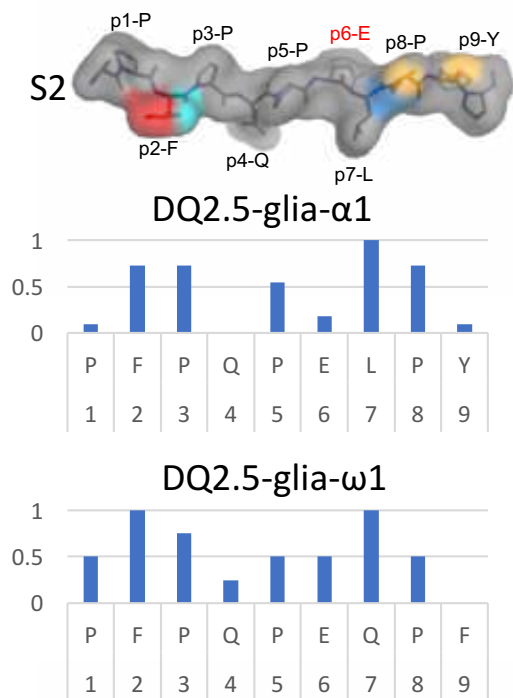
- 767 1. Trowsdale, J. & Knight, J.C. Major histocompatibility complex genomics and human disease.
768 *Annu Rev Genomics Hum Genet* **14**, 301-23 (2013).
- 769 2. Dendrou, C.A., Petersen, J., Rossjohn, J. & Fugger, L. HLA variation and disease. *Nat Rev*
770 *Immunol* **18**, 325-339 (2018).
- 771 3. Pollard, K.M., Hultman, P. & Kono, D.H. Toxicology of autoimmune diseases. *Chem Res*
772 *Toxicol* **23**, 455-66 (2010).
- 773 4. Marino, E. et al. Gut microbial metabolites limit the frequency of autoimmune T cells and
774 protect against type 1 diabetes. *Nat Immunol* **18**, 552-562 (2017).
- 775 5. Li, B., Selmi, C., Tang, R., Gershwin, M.E. & Ma, X. The microbiome and autoimmunity: a
776 paradigm from the gut-liver axis. *Cell Mol Immunol* **15**, 595-609 (2018).
- 777 6. Sollid, L.M. & Jabri, B. Triggers and drivers of autoimmunity: lessons from coeliac disease.
778 *Nat Rev Immunol* **13**, 294-302 (2013).
- 779 7. Sollid, L.M., Qiao, S.W., Anderson, R.P., Gianfrani, C. & Koning, F. Nomenclature and listing
780 of celiac disease relevant gluten T-cell epitopes restricted by HLA-DQ molecules.
781 *Immunogenetics* **64**, 455-60 (2012).
- 782 8. Tye-Din, J.A. et al. Comprehensive, quantitative mapping of T cell epitopes in gluten in
783 celiac disease. *Sci Transl Med* **2**, 41ra51 (2010).
- 784 9. Kim, C.Y., Quarsten, H., Bergseng, E., Khosla, C. & Sollid, L.M. Structural basis for HLA-DQ2-
785 mediated presentation of gluten epitopes in celiac disease. *Proc Natl Acad Sci U S A* **101**,
786 4175-9 (2004).
- 787 10. Henderson, K.N. et al. A structural and immunological basis for the role of human
788 leukocyte antigen DQ8 in celiac disease. *Immunity* **27**, 23-34 (2007).
- 789 11. Molberg, O. et al. Tissue transglutaminase selectively modifies gliadin peptides that are
790 recognized by gut-derived T cells in celiac disease. *Nat Med* **4**, 713-7 (1998).
- 791 12. Qiao, S.W. et al. Posttranslational modification of gluten shapes TCR usage in celiac
792 disease. *J Immunol* **187**, 3064-71 (2011).
- 793 13. Broughton, S.E. et al. Biased T cell receptor usage directed against human leukocyte
794 antigen DQ8-restricted gliadin peptides is associated with celiac disease. *Immunity* **37**, 611-
795 21 (2012).
- 796 14. Petersen, J. et al. T-cell receptor recognition of HLA-DQ2-gliadin complexes associated with
797 celiac disease. *Nat Struct Mol Biol* **21**, 480-8 (2014).
- 798 15. Qiao, S.W., Christophersen, A., Lundin, K.E. & Sollid, L.M. Biased usage and preferred
799 pairing of alpha- and beta-chains of TCRs specific for an immunodominant gluten epitope
800 in coeliac disease. *Int Immunol* **26**, 13-9 (2014).
- 801 16. Vriezinga, S.L. et al. Randomized Feeding Intervention in Infants at High Risk for Celiac
802 Disease. *New England Journal of Medicine* **371**, 1304-1315 (2014).
- 803 17. Marild, K., Kahrs, C.R., Tapia, G., Stene, L.C. & Stordal, K. Infections and risk of celiac
804 disease in childhood: a prospective nationwide cohort study. *Am J Gastroenterol* **110**,
805 1475-84 (2015).
- 806 18. Viitasalo, L. et al. Early microbial markers of celiac disease. *J Clin Gastroenterol* **48**, 620-4
807 (2014).
- 808 19. Ludvigsson, J.F. & Murray, J.A. Epidemiology of Celiac Disease. *Gastroenterol Clin North Am*
809 **48**, 1-18 (2019).

- 810 20. Kagnoff, M.F. et al. Evidence for the role of a human intestinal adenovirus in the
811 pathogenesis of coeliac disease. *Gut* **28**, 995-1001 (1987).
- 812 21. Kagnoff, M.F., Austin, R.K., Hubert, J.J., Bernardin, J.E. & Kasarda, D.D. Possible role for a
813 human adenovirus in the pathogenesis of celiac disease. *J Exp Med* **160**, 1544-57 (1984).
- 814 22. Dahal-Koirala, S. et al. Discriminative T-cell receptor recognition of highly homologous HLA-
815 DQ2-bound gluten epitopes. *J Biol Chem* **294**, 941-952 (2019).
- 816 23. Purcell, A.W., Ramarathinam, S.H. & Ternette, N. Mass spectrometry-based identification
817 of MHC-bound peptides for immunopeptidomics. *Nat Protoc* **14**, 1687-1707 (2019).
- 818 24. Anderson, R.P., Degano, P., Godkin, A.J., Jewell, D.P. & Hill, A.V.S. In vivo antigen challenge
819 in celiac disease identifies a single transglutaminase-modified peptide as the dominant A-
820 gliadin T-cell epitope. *Nat Med* **6**, 337-342 (2000).
- 821 25. Verdu, E.F., Galipeau, H.J. & Jabri, B. Novel players in coeliac disease pathogenesis: role of
822 the gut microbiota. *Nat Rev Gastroenterol Hepatol* **12**, 497-506 (2015).
- 823 26. Stene, L.C. et al. Rotavirus infection frequency and risk of celiac disease autoimmunity in
824 early childhood: a longitudinal study. *Am J Gastroenterol* **101**, 2333-40 (2006).
- 825 27. Bouziat, R. et al. Reovirus infection triggers inflammatory responses to dietary antigens and
826 development of celiac disease. *Science* **356**, 44-50 (2017).
- 827 28. Kahrs, C.R. et al. Enterovirus as trigger of coeliac disease: nested case-control study within
828 prospective birth cohort. *BMJ* **364**, l231 (2019).
- 829 29. Ashorn, S. et al. Elevated serum anti-Saccharomyces cerevisiae, anti-I2 and anti-OmpW
830 antibody levels in patients with suspicion of celiac disease. *J Clin Immunol* **28**, 486-94
831 (2008).
- 832 30. Riddle, M.S., Murray, J.A. & Porter, C.K. The incidence and risk of celiac disease in a healthy
833 US adult population. *Am J Gastroenterol* **107**, 1248-55 (2012).
- 834 31. Riddle, M.S., Murray, J.A., Cash, B.D., Pimentel, M. & Porter, C.K. Pathogen-specific risk of
835 celiac disease following bacterial causes of foodborne illness: a retrospective cohort study.
836 *Dig Dis Sci* **58**, 3242-5 (2013).
- 837 32. Sanchez, E., Donat, E., Ribes-Koninckx, C., Fernandez-Murga, M.L. & Sanz, Y. Duodenal-
838 mucosal bacteria associated with celiac disease in children. *Appl Environ Microbiol* **79**,
839 5472-9 (2013).
- 840 33. Wacklin, P. et al. Altered duodenal microbiota composition in celiac disease patients
841 suffering from persistent symptoms on a long-term gluten-free diet. *Am J Gastroenterol*
842 **109**, 1933-41 (2014).
- 843 34. Viitasalo, L. et al. Microbial Biomarkers in Patients with Nonresponsive Celiac Disease. *Dig*
844 *Dis Sci* **63**, 3434-3441 (2018).
- 845 35. D'Argenio, V. et al. Metagenomics Reveals Dysbiosis and a Potentially Pathogenic *N.*
846 *flavescens* Strain in Duodenum of Adult Celiac Patients. *Am J Gastroenterol* **111**, 879-90
847 (2016).
- 848 36. Caminero, A. et al. Duodenal Bacteria From Patients With Celiac Disease and Healthy
849 Subjects Distinctly Affect Gluten Breakdown and Immunogenicity. *Gastroenterology* **151**,
850 670-83 (2016).
- 851 37. Caminero, A. et al. Duodenal bacterial proteolytic activity determines sensitivity to dietary
852 antigen through protease-activated receptor-2. *Nat Commun* **10**, 1198 (2019).
- 853 38. Dickson, R.P. et al. Cell-associated bacteria in the human lung microbiome. *Microbiome* **2**,
854 28 (2014).
- 855 39. N'Diaye, A. et al. Substance P and Calcitonin Gene-Related Peptide: Key Regulators of
856 Cutaneous Microbiota Homeostasis. *Front Endocrinol (Lausanne)* **8**, 15 (2017).

- 857 40. Scales, B.S., Dickson, R.P., LiPuma, J.J. & Huffnagle, G.B. Microbiology, genomics, and
858 clinical significance of the *Pseudomonas fluorescens* species complex, an unappreciated
859 colonizer of humans. *Clin Microbiol Rev* **27**, 927-48 (2014).
- 860 41. Dalwadi, H., Wei, B., Kronenberg, M., Sutton, C.L. & Braun, J. The Crohn's disease-
861 associated bacterial protein I2 is a novel enteric t cell superantigen. *Immunity* **15**, 149-58
862 (2001).
- 863 42. Sutton, C.L. et al. Identification of a novel bacterial sequence associated with Crohn's
864 disease. *Gastroenterology* **119**, 23-31 (2000).
- 865 43. Segal, Y. & Shoenfeld, Y. Vaccine-induced autoimmunity: the role of molecular mimicry and
866 immune crossreaction. *Cell Mol Immunol* **15**, 586-594 (2018).
- 867 44. Lang, H.L. et al. A functional and structural basis for TCR cross-reactivity in multiple
868 sclerosis. *Nat Immunol* **3**, 940-3 (2002).
- 869 45. Cole, D.K. et al. Hotspot autoimmune T cell receptor binding underlies pathogen and
870 insulin peptide cross-reactivity. *The Journal of Clinical Investigation* **126**, 3626-3626 (2016).
- 871 46. Kabsch, W. Xds. *Acta Crystallogr D Biol Crystallogr* **66**, 125-32 (2010).
- 872 47. Winn, M.D. et al. Overview of the CCP4 suite and current developments. *Acta Crystallogr D*
873 *Biol Crystallogr* **67**, 235-42 (2011).
- 874 48. McCoy, A.J. et al. Phaser crystallographic software. *J Appl Crystallogr* **40**, 658-674 (2007).
- 875 49. Emsley, P., Lohkamp, B., Scott, W.G. & Cowtan, K. Features and development of Coot. *Acta*
876 *Crystallogr D Biol Crystallogr* **66**, 486-501 (2010).
- 877 50. Adams, P.D. et al. PHENIX: a comprehensive Python-based system for macromolecular
878 structure solution. *Acta Crystallogr D Biol Crystallogr* **66**, 213-21 (2010).
- 879 51. Gras, S. et al. Allelic polymorphism in the T cell receptor and its impact on immune
880 responses. *J Exp Med* **207**, 1555-67 (2010).
- 881

Figure 1

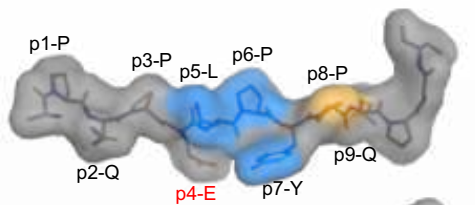
a



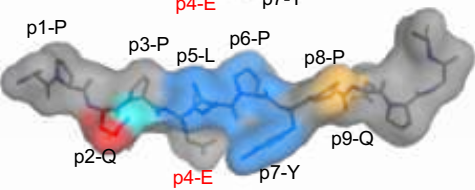
b

Peptide	sequence
DQ2.5-glia-α1	<u>LQPFQPELPY</u>
<i>DQ2.5-B.fragil-α1a</i>	KELPQPELPYS
<i>DQ2.5-B.pyogen-α1a</i>	PPLPQPEVPET
<i>DQ2.5-P.fluor-α1a</i>	PMPMPELPYP
<i>DQ2.5-P.fluor-α1b</i>	PMPLPDLPYYP
<i>DQ2.5-P.fluor-α1c</i>	VNYPHPDVPLYT
<i>DQ2.5-A.baum-α1.a</i>	VQPWPQPELPEY
<i>DQ2.5-B.petri-α1a</i>	PYTLP E LPYDA
<i>DQ2.5-Clost.sp-α1a</i>	LPYPQPELPGV
<i>DQ2.5-S.cerev-α1a</i>	RYMPDPELPYI
<i>DQ2.5-M.smith-α1a</i>	DVFKVEPEIPY
DQ2.5-glia-ω1	<u>PFQPEQPF</u>
<i>DQ2.5-P.fluor-ω1a</i>	PPLPEPEQPPV
<i>DQ2.5-E.cloac-ω1a</i>	PPFPEGEQPPF
<i>DQ2.5-A.baum-ω1a</i>	SQPIPQPEQPP
DQ2.5-glia-α2	<u>FQPELPYPQP</u>
<i>DQ2.5-P.fluor-α2a</i>	PMP E LPYPAT
<i>DQ2.5-P.fluor-α2b</i>	PLP E LPYPAT
<i>DQ2.5-P.fluor-α2c</i>	NPPPDLPYPDI
<i>DQ2.5-B.fragil-α2a</i>	LPQPELPYSEM
<i>DQ2.5-B.copro-α2a</i>	LPLPDLPYPVA
<i>DQ2.5-S.fonti-α2a</i>	LPLP E LPYSQP
<i>DQ2.5-P.aerug-α2a</i>	MVVQSELPYPE
<i>DQ2.5-S.cerev-α2a</i>	MPDPELPYINL
<i>DQ2.5-M.smith-α2a</i>	KVEPEIPYPED
<i>DQ2.5-B.cereus-α2a</i>	KPQPEQPKPQP

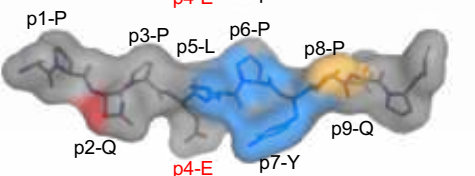
JR5.1



S16



D2



DQ2.5-glia- α 2

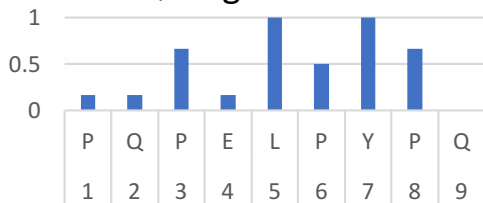
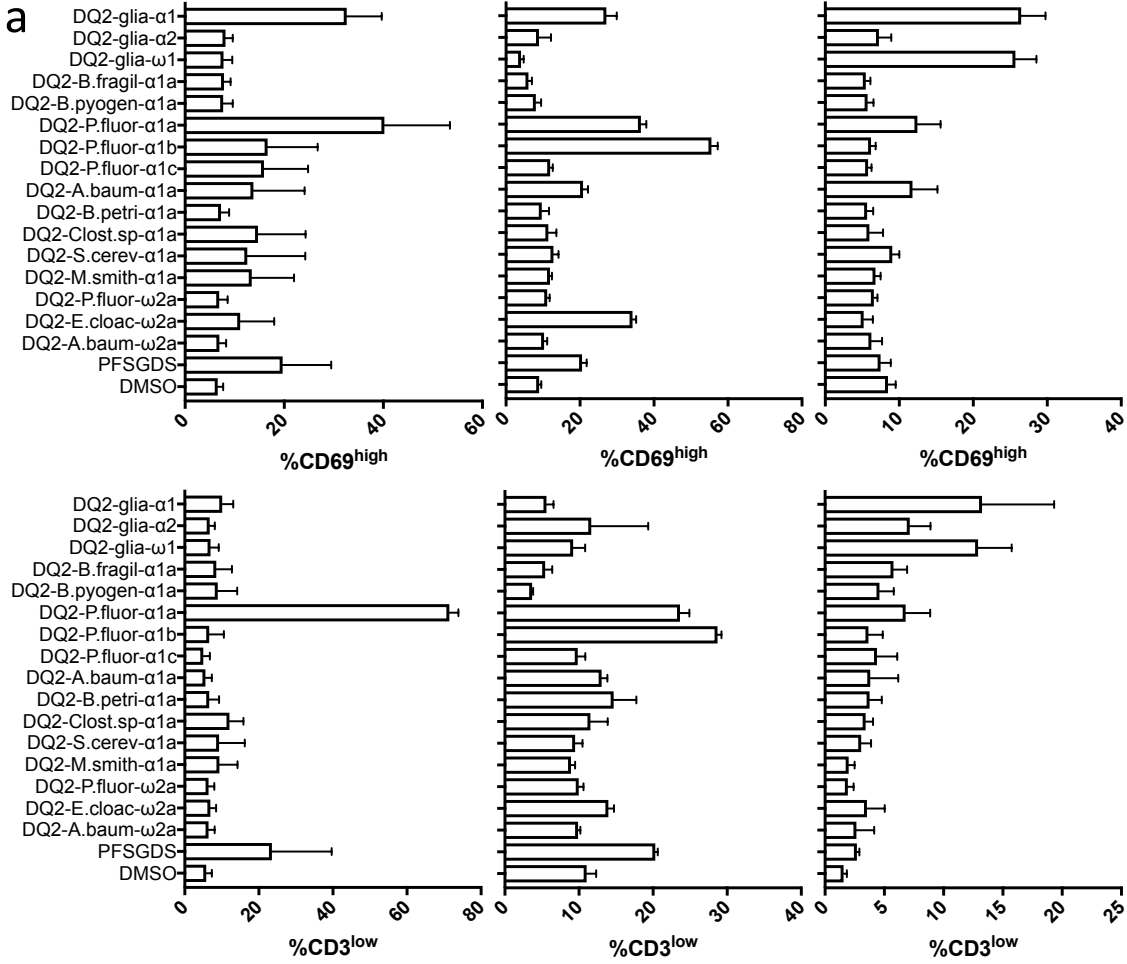


Figure 2:

LS2.8/3.15

N12

L6



b

JR5.1

S16

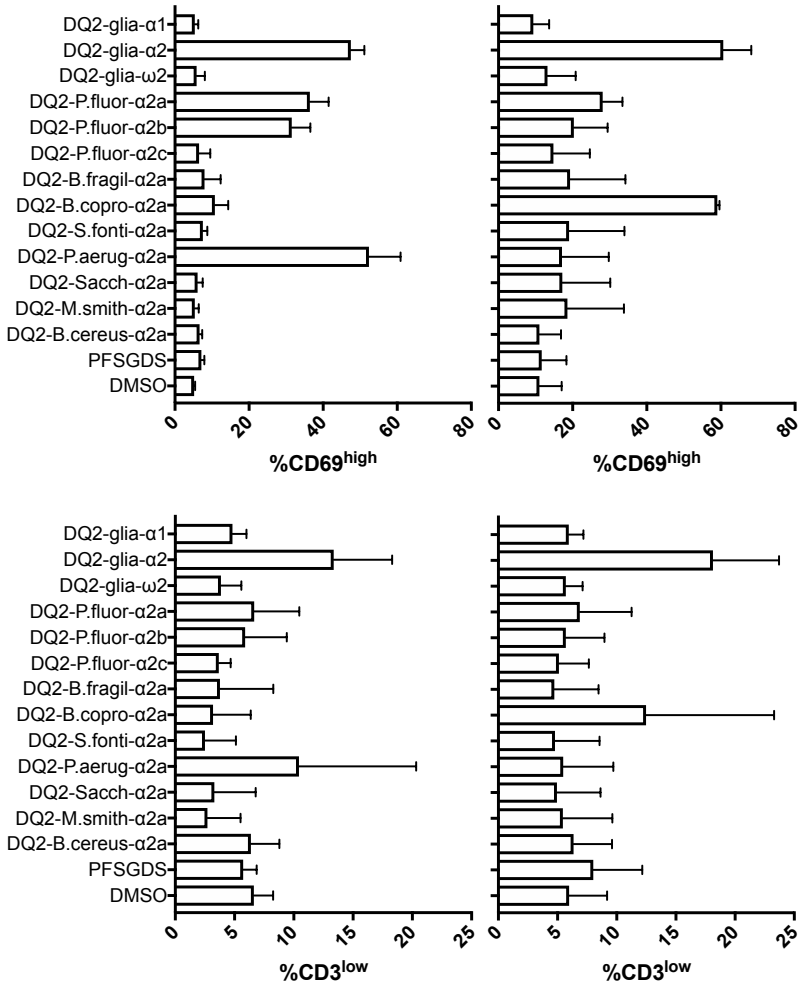


Figure 3

a

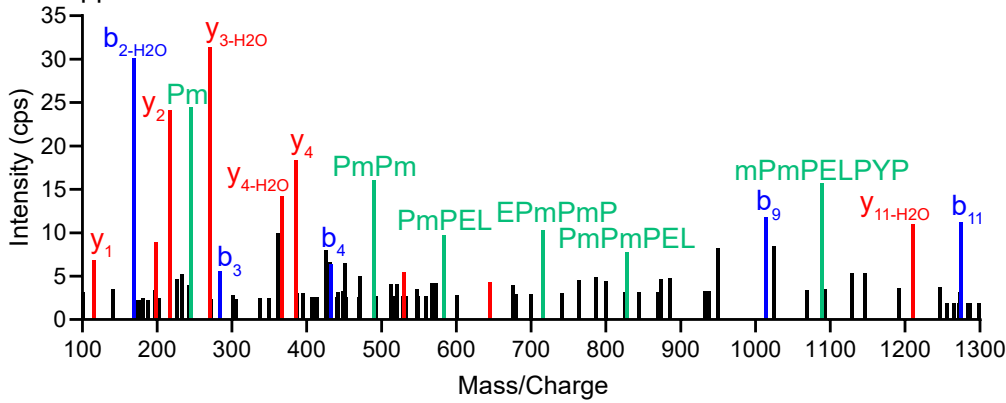
Succinylglutamate desuccinylase



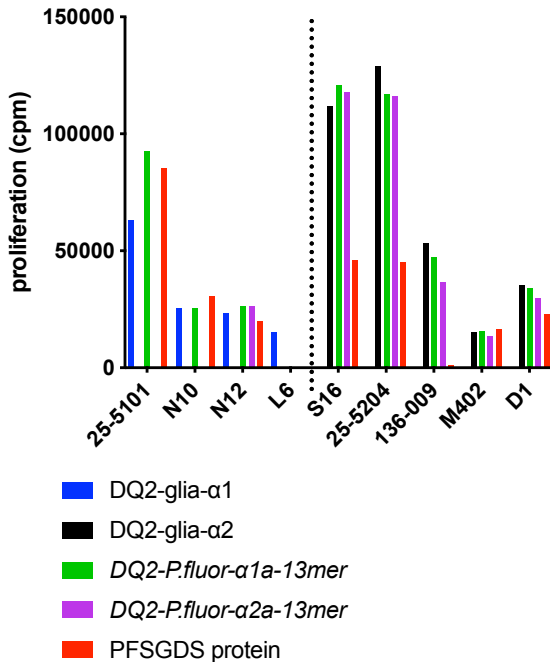
b

GEPmPmPELPYPATP (from 9022 DQ2 cells)

precursor m/z = 829.8730
 ppm = -1.9



c



d

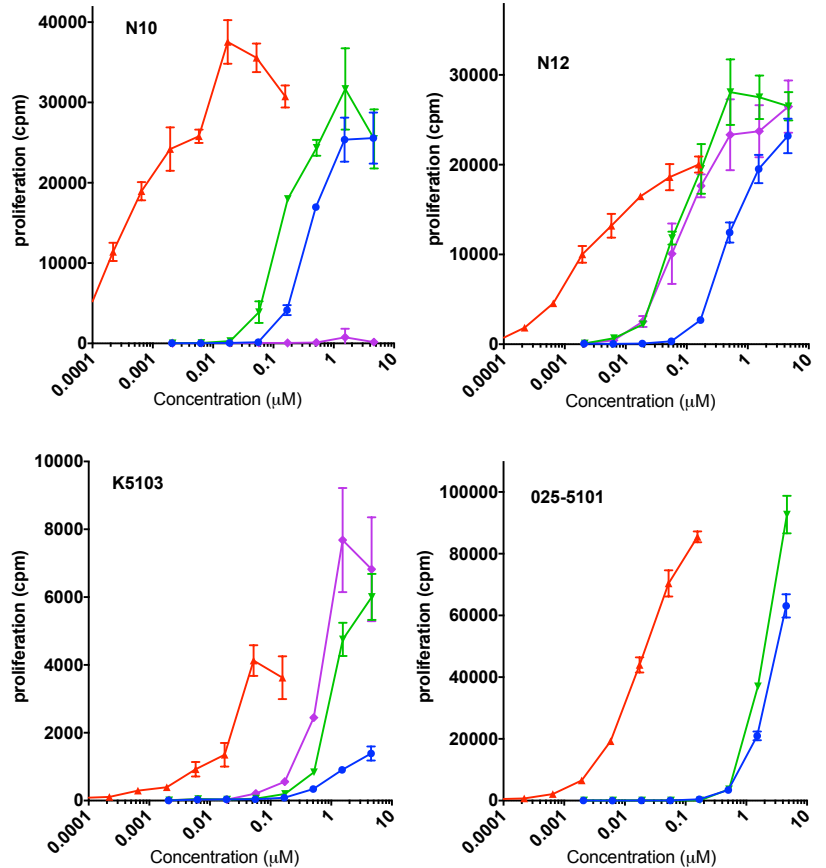


Figure 4

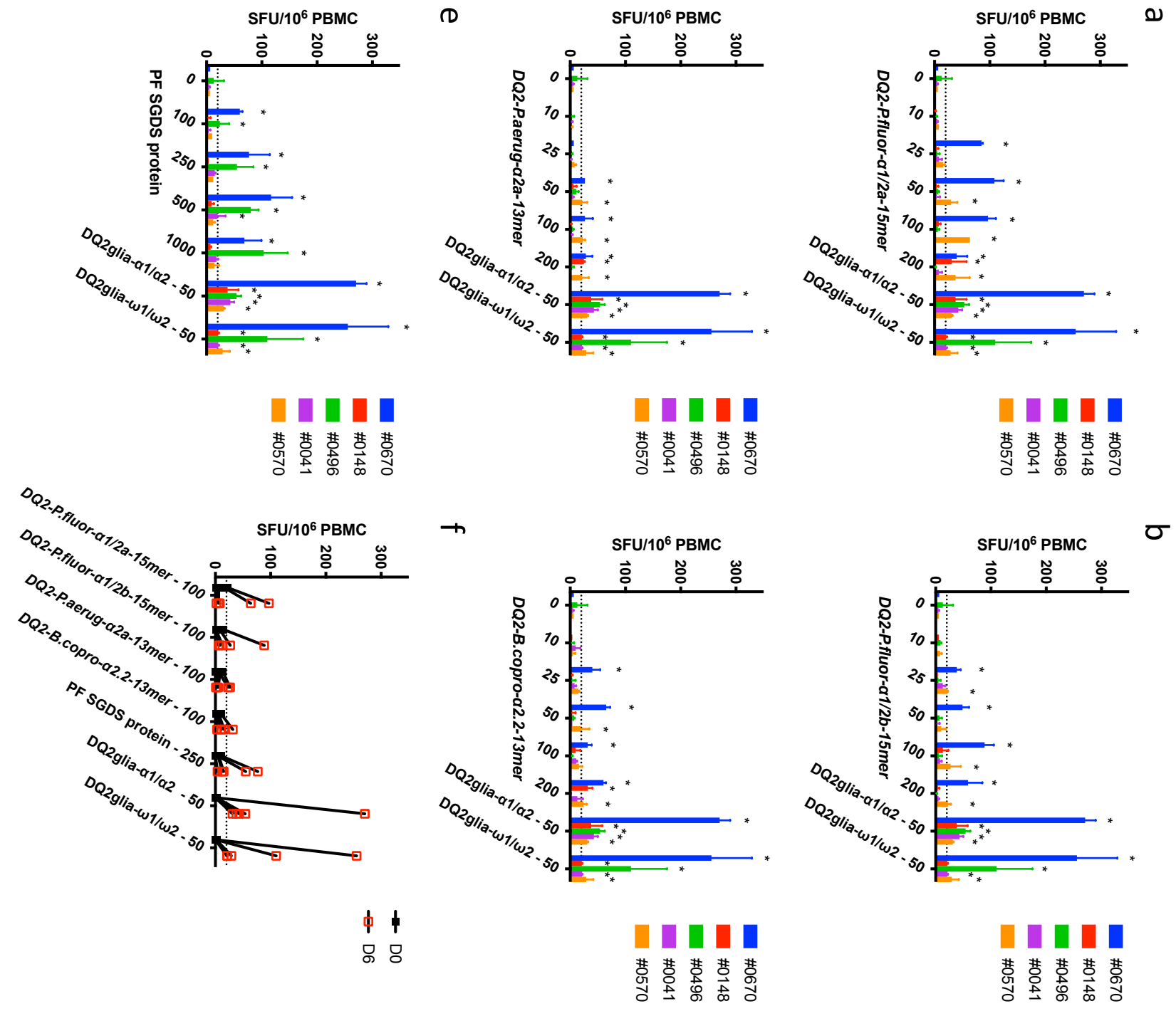
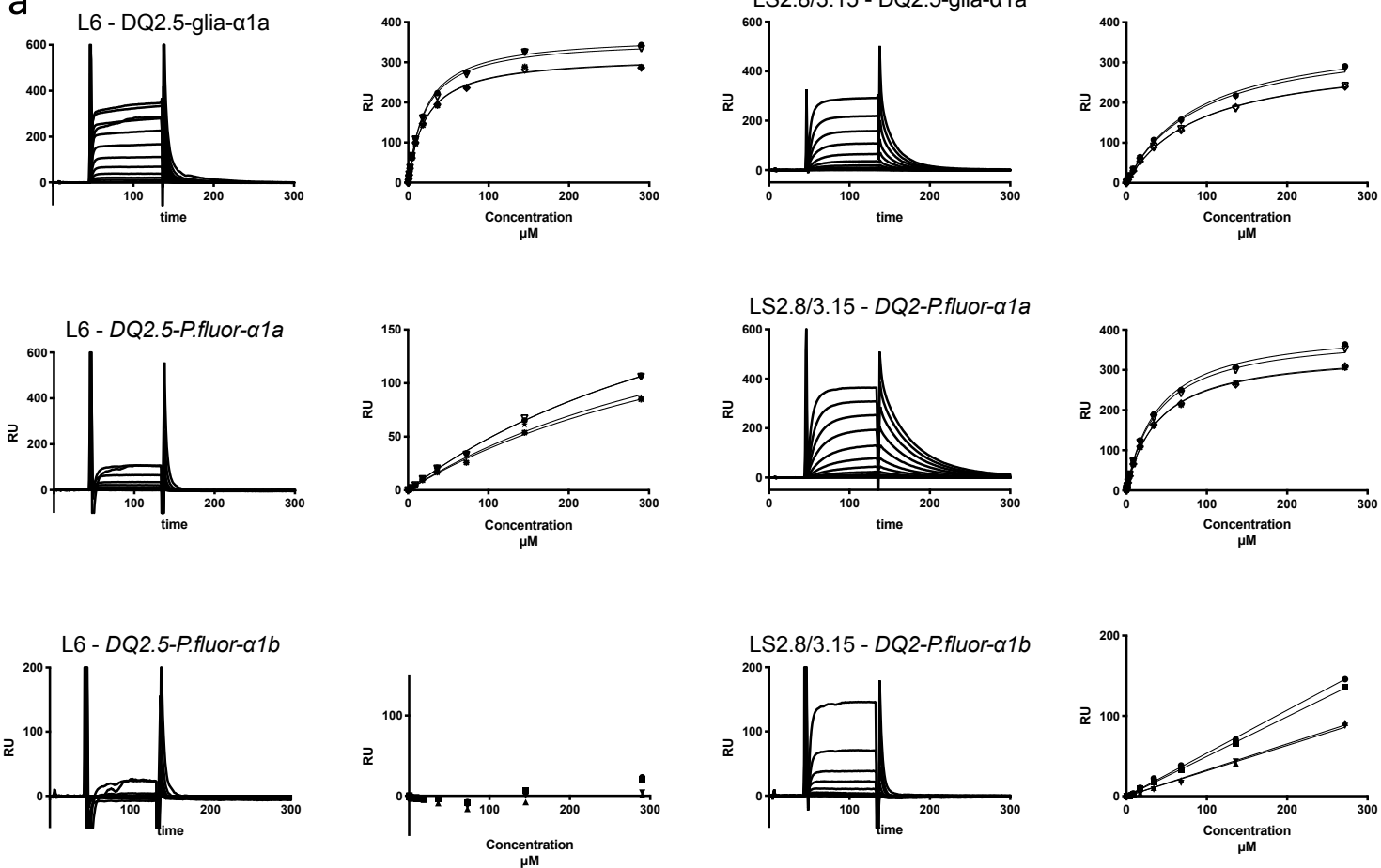


Figure 5

a



b

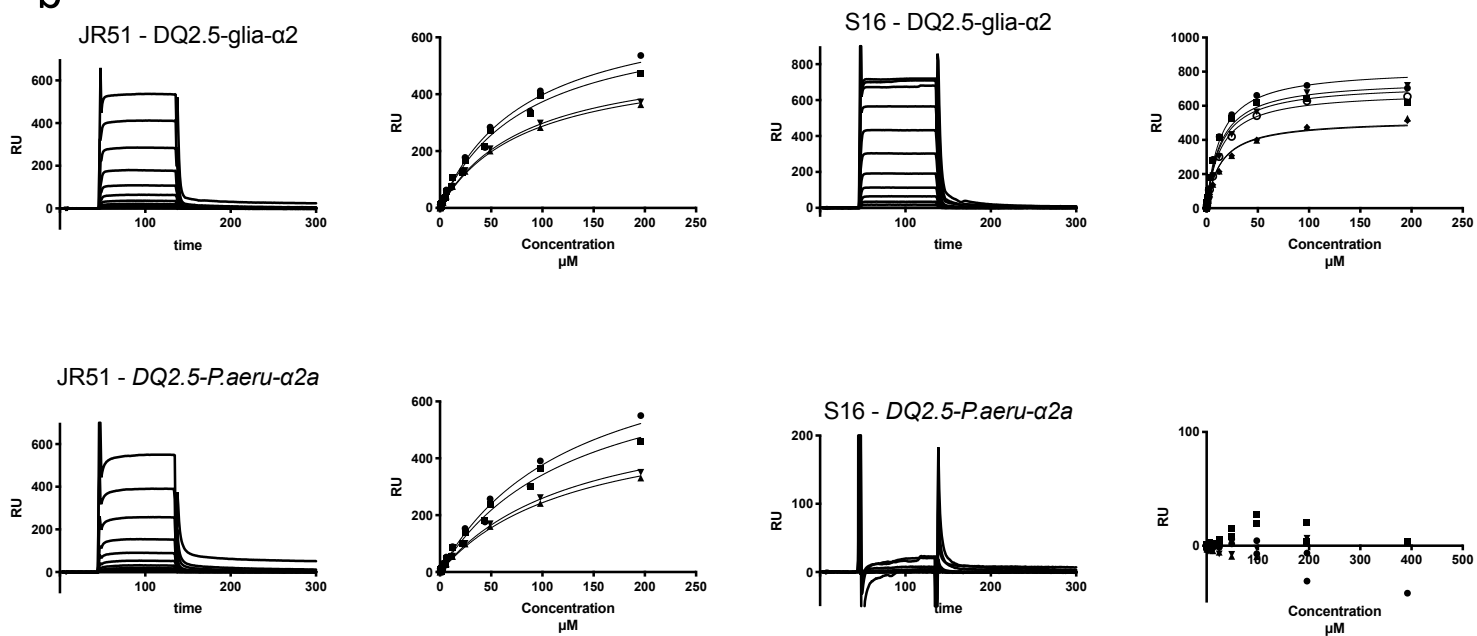
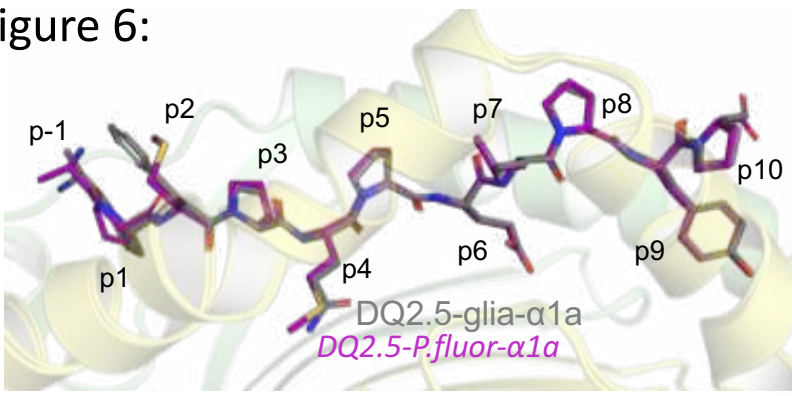
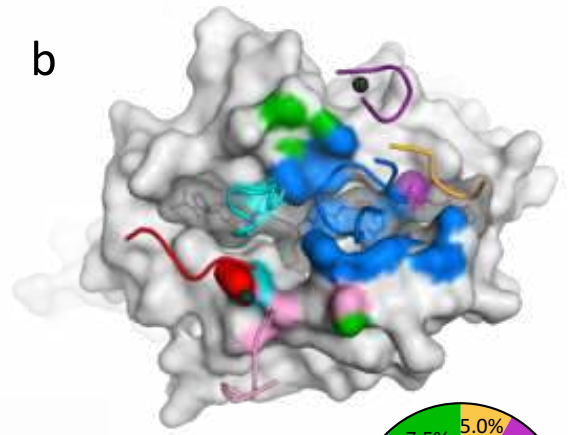


Figure 6:

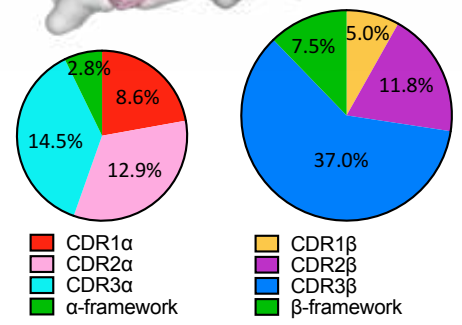
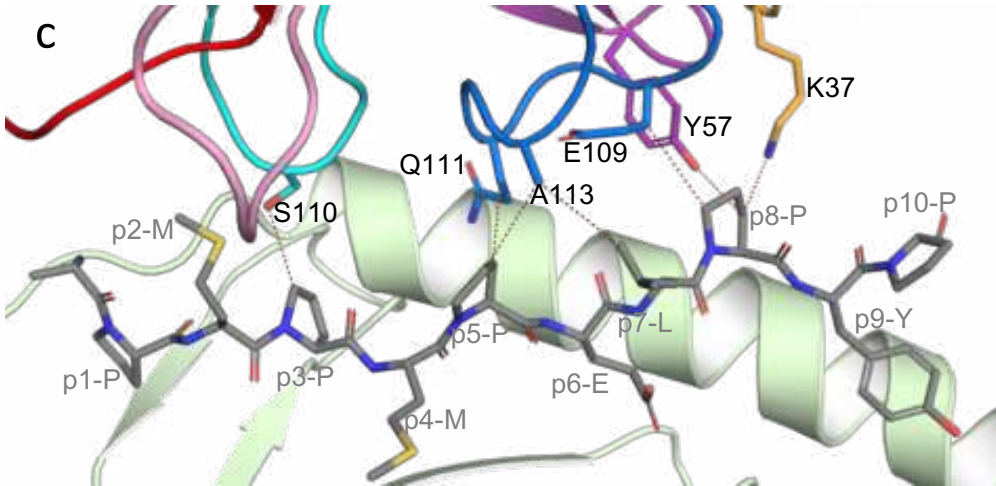
a



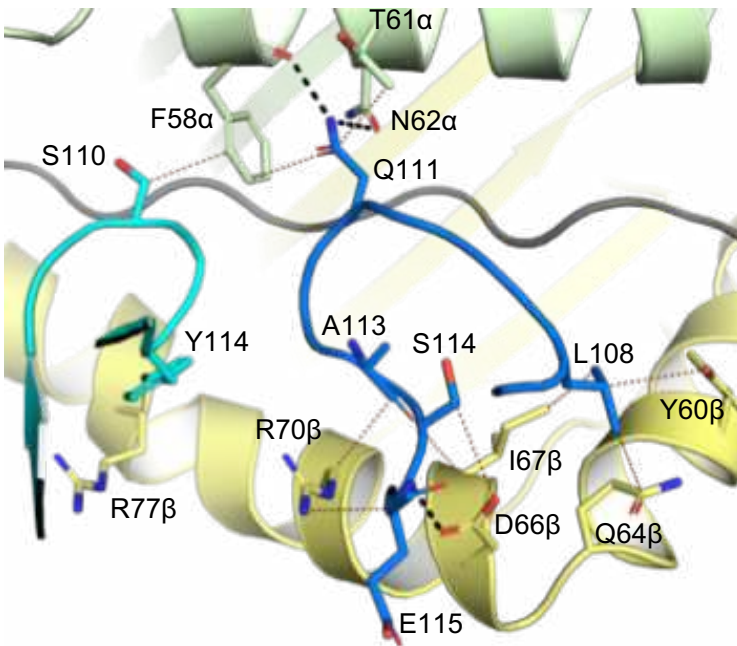
b



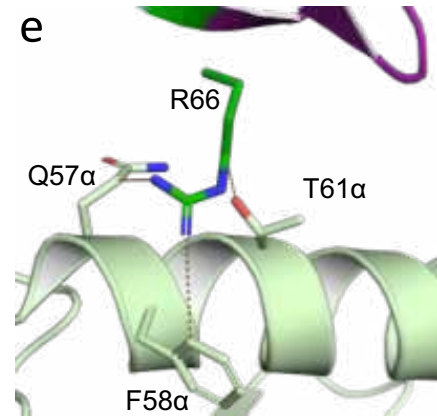
c



d



e



f

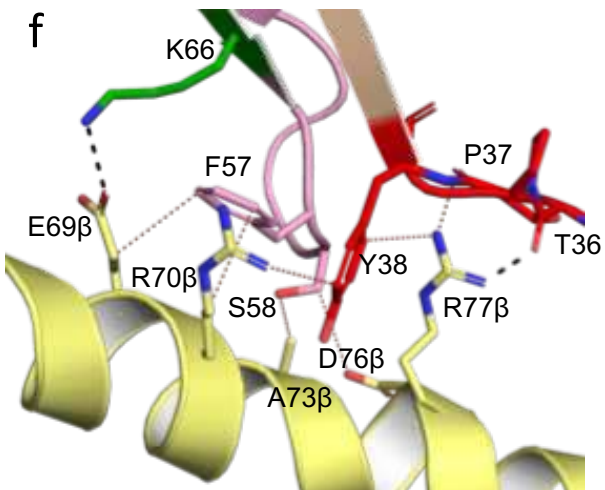
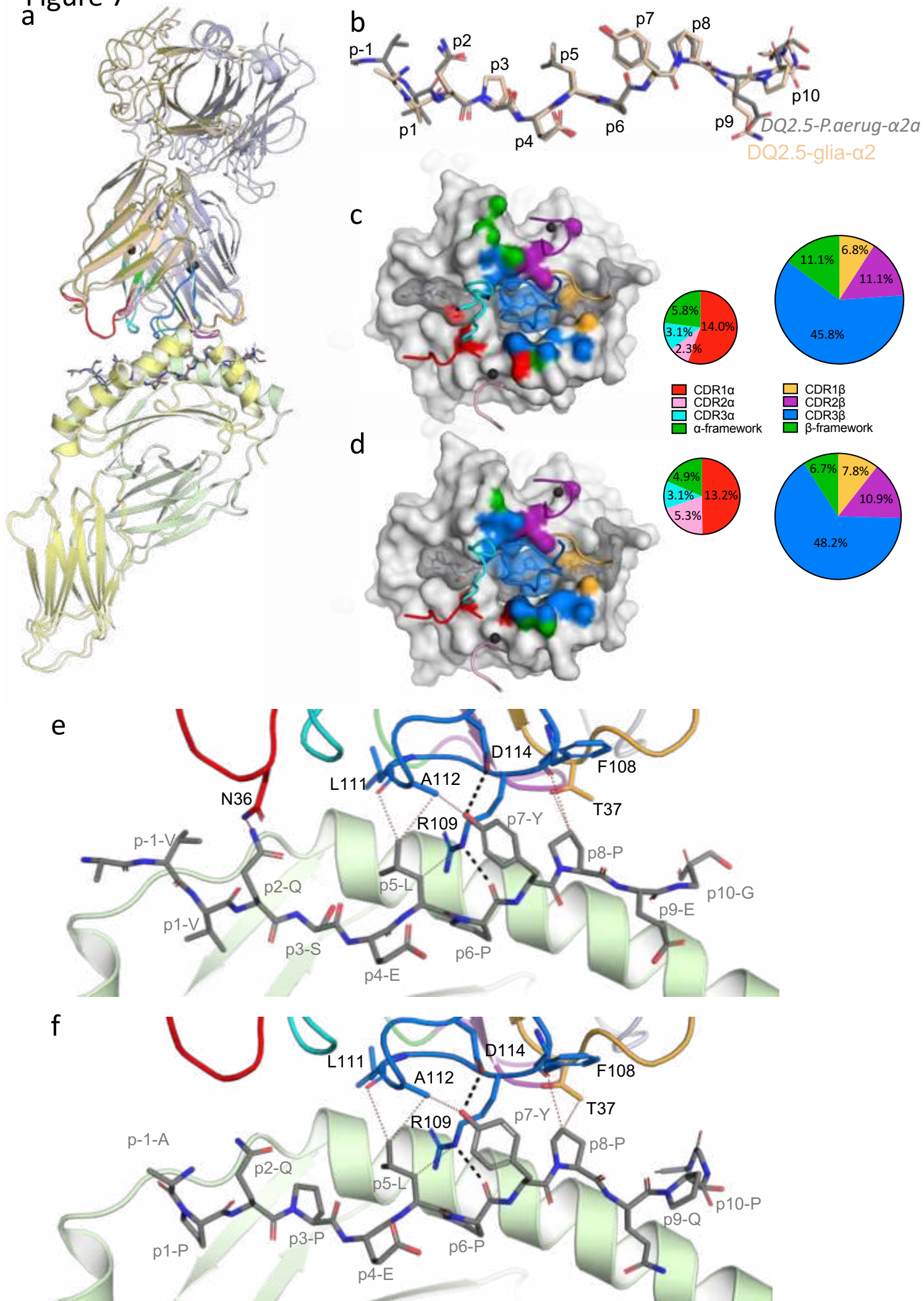
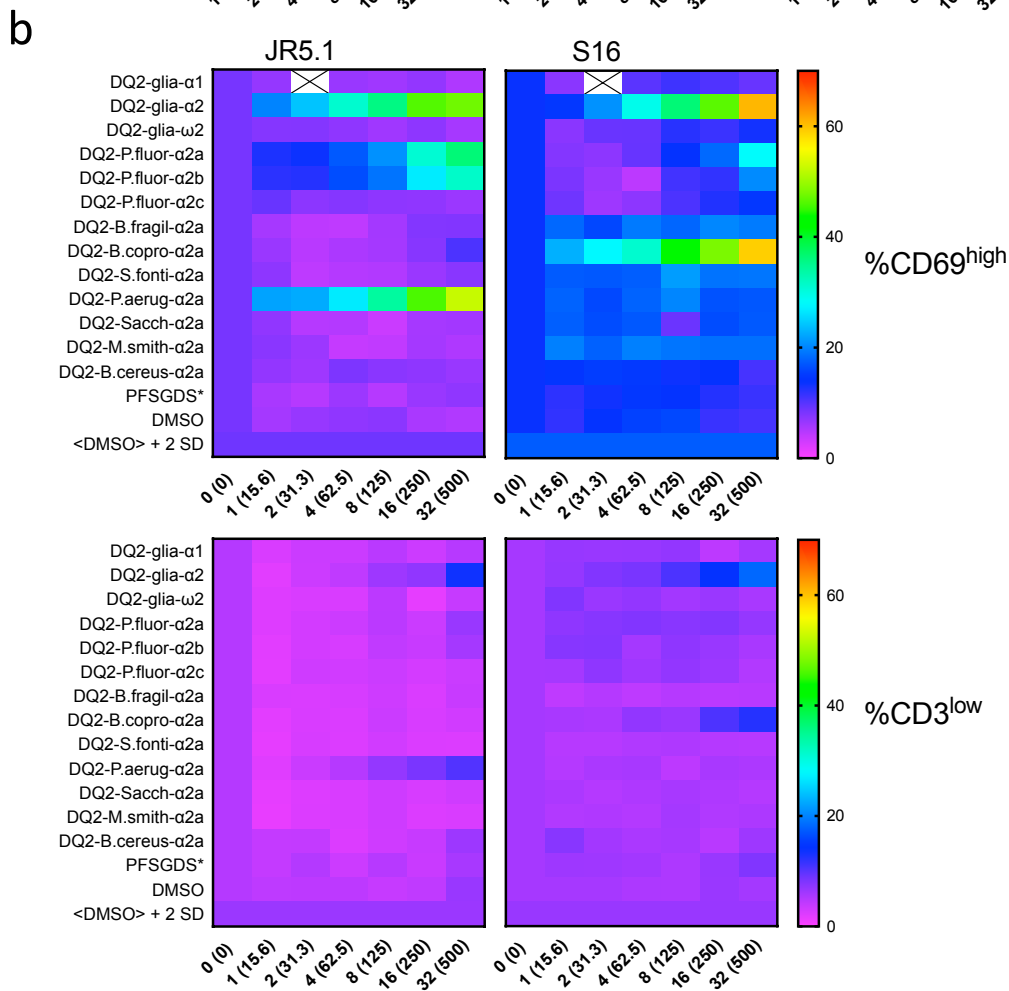
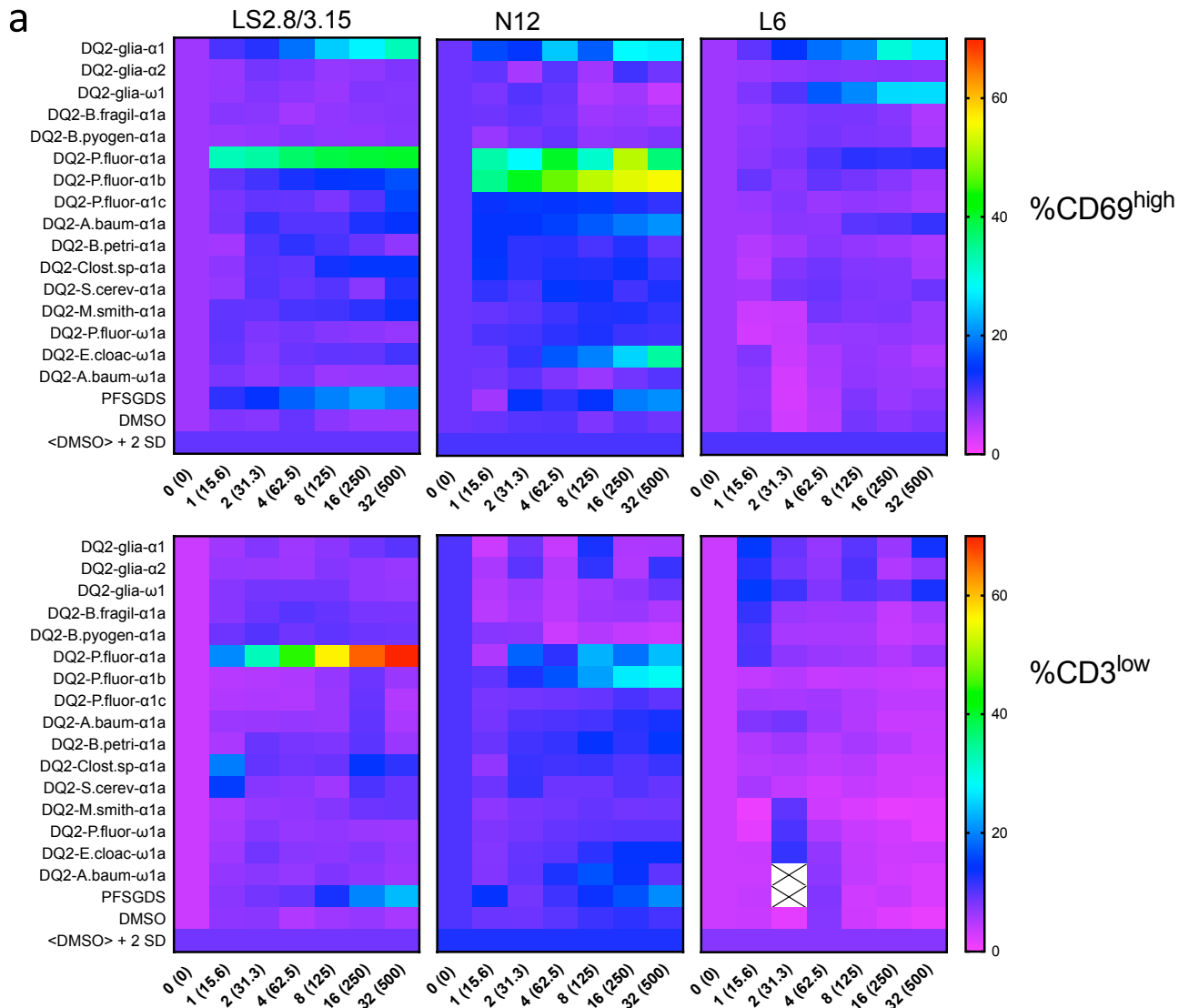


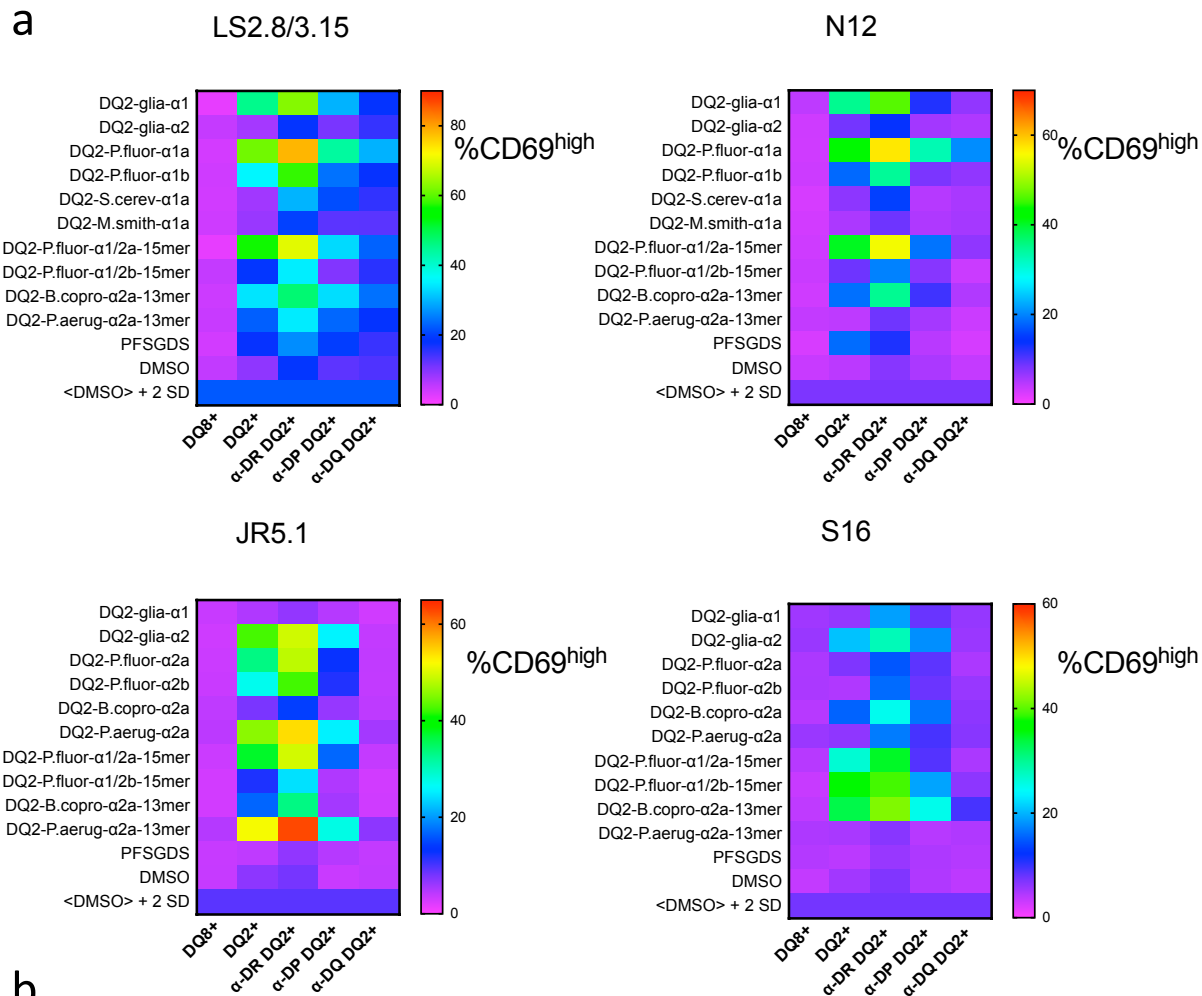
Figure 7



Supp. Figure 1



Supp. Figure 2



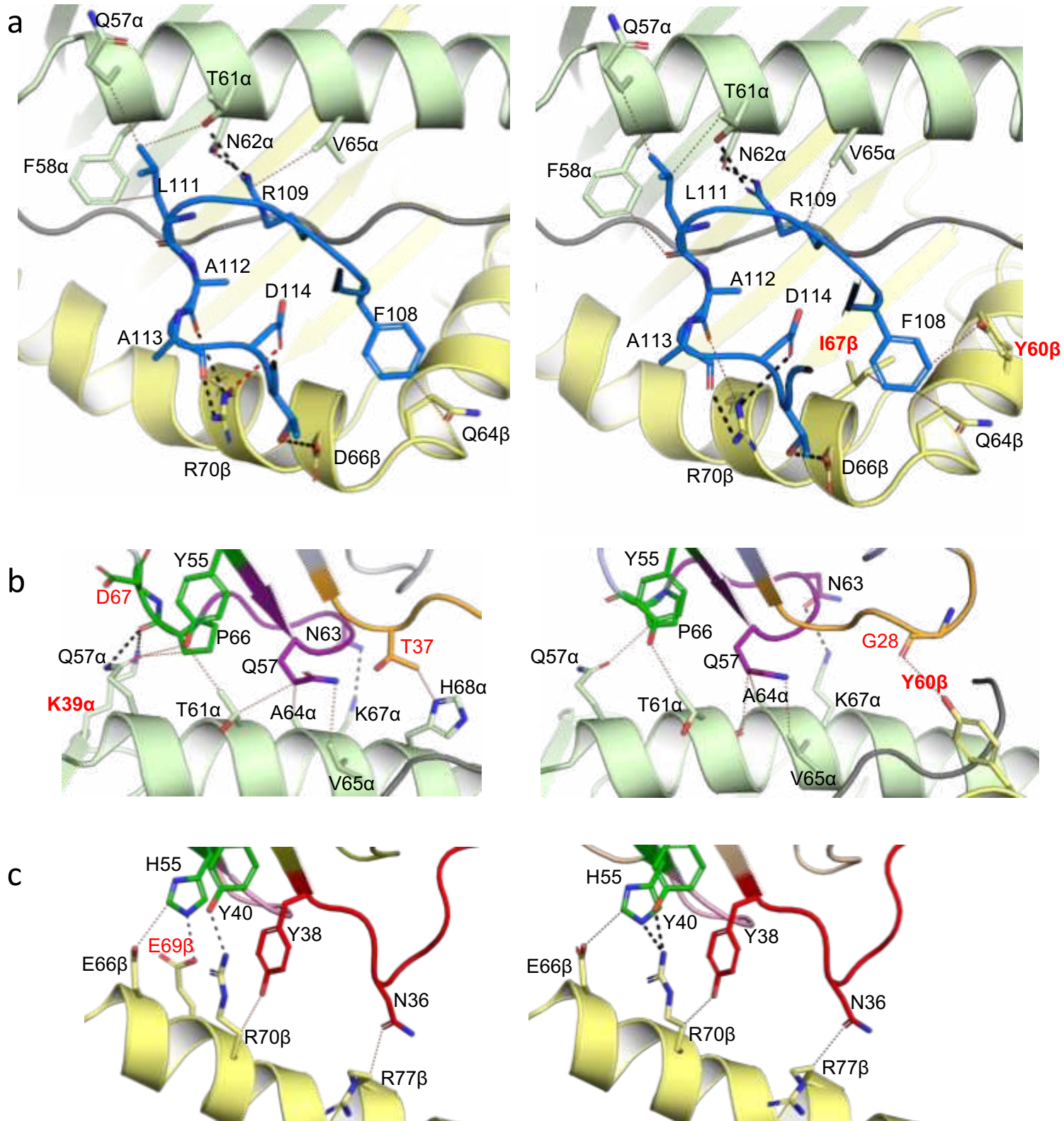
b

Peptide	sequence
DQ2.5-glia-α1	LQPFQPELPY
DQ2.5-glia-α2	FPQPELPYPQ
<i>DQ2.5-P.fluor-α1a</i>	PMPMPELPYP
<i>DQ2.5-P.fluor-α2a</i>	PMPPELPYPAT
<i>DQ2.5-P.fluor-α1a-13mer</i>	GEPMPMPELPYPA
<i>DQ2.5-P.fluor-α2a-13mer</i>	PMPMPELPYPATP
<i>DQ2.5-P.fluor-α1/α2a-15mer</i>	GEPMPMPELPYPATP
<i>DQ2.5-P.fluor-α1b</i>	PMPLPDLPYP
<i>DQ2.5-P.fluor-α2c</i>	PLPELPYPAT
<i>DQ2.5-P.fluor-α1/α2b-15mer</i>	GEPMLPLPDLPYPATP
<i>DQ2.5-P.aerug-α2a</i>	MVVQSELPYPE
<i>DQ2.5-P.aerug-α2a-13mer</i>	MVVQSELPYPEGV
<i>DQ2.5-B.copro-α2.2</i>	LPLPDLPYPVA
<i>DQ2.5-B.copro-α2.2-13mer</i>	WLPLPDLPYPVAY
DQ2.5-glia-α1a/α2-15mer	LQPFQPELPYPQ
DQ2.5-glia-ω1/ω2 -15mer	QPFQPEQFPWQP

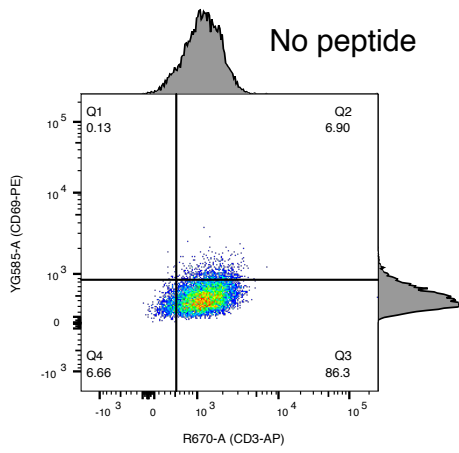
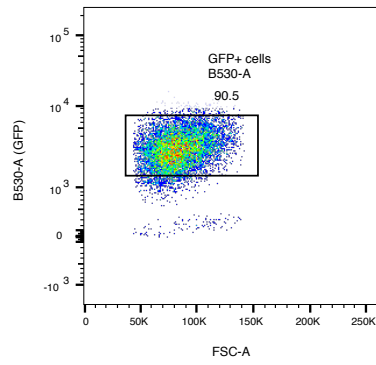
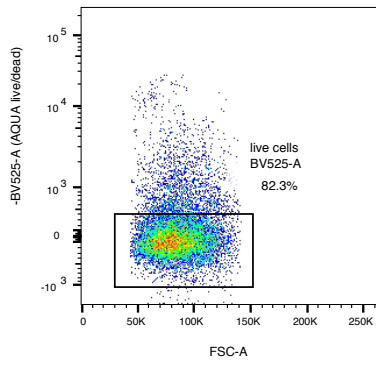
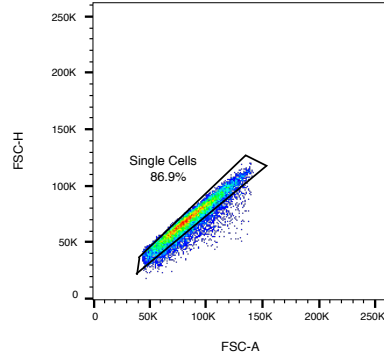
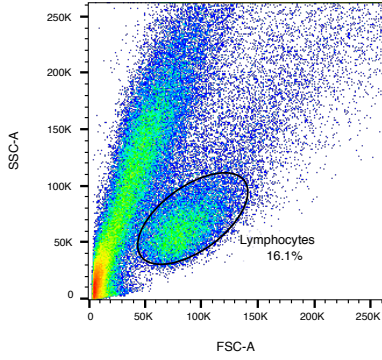
Supp. Figure 3



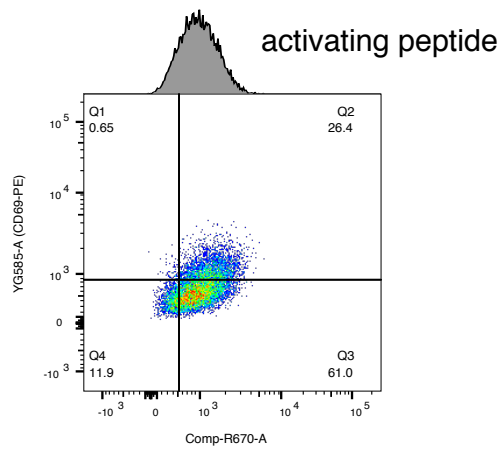
Supp. Figure 4



Supp. Figure 5



E11
FSC-A, Comp-B530-A subset
8257



C02
FSC-A, Comp-B530-A subset
8934